



Coral reef, Funafuti, Tuvalu

Chapter 3

Observed Climate Variability and Trends

Summary

The IPCC Fourth Assessment Report (Hegerl et al., 2007) concluded that “anthropogenic warming of the climate system can be detected in temperature observations taken at the surface, in the troposphere and in the oceans”, and that “greenhouse gas forcing has very likely caused most of the observed global warming over the last 50 years”.

Studies also show that zonal average warming in the tropics and sub-tropics over the period 1901–2005 (Hegerl et al., 2007) is not reproduced in climate models with natural variability alone, but can be reproduced in climate models that include anthropogenic forcing incorporating increases in greenhouse gases.

- Collectively, the observed climate record of the PCCSP region indicates a climate in transition, driven by both natural and human influences.
- Palaeoclimate records indicate the Pacific is characterised by climate variability on a wide variety of time scales. Changes in the frequency and intensity of El Niño–Southern Oscillation (ENSO) activity over the past 12 000 years have been linked to widespread changes in climate impacts.
- Natural climate oscillations, e.g. ENSO, the Pacific Decadal Oscillation (PDO), the Interdecadal Pacific Oscillation (IPO), Southern Annular Mode (SAM), the Indian Ocean Dipole (IOD), and fluctuations in the key climatological features of the region (Intertropical Convergence Zone (ITCZ), South Pacific Convergence Zone (SPCZ), and West Pacific Monsoon (WPM)) are responsible for much of the variability in the atmosphere and ocean on seasonal to multi-decadal timescales.
- Temperature records from Pacific Island observation stations show a clear signal of warming over the past 50 years, with most stations warming at a rate between +0.08 and +0.20°C per decade over this time, consistent with global trends.
- Rainfall across the region has increased and decreased in response to natural climate variability. Over the past 50 years, rainfall totals increased to the north-east of the SPCZ, and declined to the south.
- There are no significant trends in the overall number of tropical cyclones, or in the number of intense tropical cyclones, in the South Pacific Ocean over the period 1981–2007. The number of severe tropical cyclones making landfall over eastern Australia has declined since the late 19th century, though this result is significant at the 90% level only.
- Sea-surface temperatures in the region have generally warmed since 1950. This warming has been partially attributed to increases in the concentration of greenhouse gases. However, temperature variations associated with the IPO/PDO also substantially influence the background trend.
- The western tropical Pacific Ocean has become significantly less salty over recent decades. Conversely, regions to the east have generally become saltier. Together, these changes suggest an intensification of the hydrological cycle.
- A distinctive pattern of intensified surface warming and sub-surface cooling, centred near a depth of 200 m is evident over the past 50 years in the Pacific Ocean. Climate models suggest this pattern is consistent with human-induced change.
- The Hadley Circulation has expanded poleward and the Walker Circulation has weakened. The weakening of the Walker Circulation over the past century is due to a combination of both natural changes and human-induced change.
- Sea level has risen globally and in the PCCSP region over recent decades. Extreme sea levels are also increasing, primarily as a result of increases in mean sea level.
- There is significant interannual variability of sea level in the region related to the ENSO cycle. Consequently, the pattern of trends in the altimeter record (since the start of satellite measurements in 1993) is not representative of longer-term trends.
- The acidity level of surface ocean waters is increasing (i.e. pH is reducing) due to the increased uptake of carbon dioxide due to the higher atmospheric concentrations that have resulted from human activities.

Anecdotally, people in the region are reporting climate change impacts, including more salt-water intrusions, changes in seasonal climate cycles, and more frequent occurrence of drought, fires, mudslides and coral bleaching (Box 3.1). However, little research has been conducted to quantify the relative importance of human-induced change and natural variability as causes of the observed trends in the PCCSP region.

3.1 Introduction

Climate variability in the PCCSP region occurs on interannual, decadal, centennial and longer time scales. Palaeoclimate records indicate that during the millennia before the Industrial Revolution (around 1750), the climate of the Pacific underwent large variations, primarily associated with changes in the intensity and frequency of the El Niño-Southern Oscillation (ENSO) (Cobb et al., 2003; Gergis and Fowler, 2009). However, in the past climate shifts were driven by natural mechanisms; it is now likely that they are also being driven by human influences (Trenberth et al., 2007).

The current way of life in the PCCSP region is based on the patterns of climate experienced over the past few centuries. The flora and fauna of the region have evolved within the climatic bounds exhibited over much longer time scales. If the mean climate shifts beyond these bounds, or changes more rapidly than seen before, many aspects of life may change. Many Pacific Islanders believe they have already seen the impacts of climate change (Box 3.1). Consequently, it is important to understand the range of climate variability experienced in the past in order to provide a context in which to interpret projections of future climate change. Understanding past variability also contributes to assessing the likely causes of climate change (discussed in Chapter 4).

This chapter summarises previous studies of observed climate variability and change in the region and describes the contributions made to this understanding by the PCCSP. The assessment of observed climate variability and change presented here is based on updated and improved meteorological and oceanographic datasets. This 'data rehabilitation' has involved significant collaboration with Partner Countries and resulted in improved data access and security, and enhanced scientific and technical capacity in the region. It is hoped that the increased knowledge and tools developed by the PCCSP will lead to improvements in the way Partner Countries manage and analyse the observational data required to detect and document climate variability and change in their respective countries.

3.2 Global Context

The evidence for global climate change is broad and compelling (Trenberth et al., 2007). Global mean surface air temperature, as determined by the HadCRUT3v global gridded dataset (Brohan et al., 2006) is estimated to have increased by 0.74°C from 1910–2010, with a trend of around 0.14°C per decade over the past 50 years (Figure 3.1). Global warming is confirmed by natural indicators such as melting glaciers and sea-ice, sea-level rise, earlier flowering and ripening dates, longer growing seasons, coral bleaching and poleward migration of plants and animals (Rosenzweig et al., 2007).

Further evidence of changes in the global climate comes from palaeoclimatic records reconstructed from sources such as ice cores,

tree rings and corals. When modern instrumental temperature records are placed in the context of reconstructed temperature records over the past 2000 years, it is apparent that the Northern Hemisphere (where sufficient palaeoclimate records exist) is currently experiencing a rapid and unusual warming (Mann et al., 2009).

A lack of data makes it difficult to reconstruct a similar long record for the Southern Hemisphere. However, global datasets based on instrumental records clearly indicate that the PCCSP region has also warmed significantly since the early 20th century (Figure 3.1). Most of the region's warmest years in the instrumental record have occurred over the past two decades. The rate of warming in the PCCSP region appears

to be slightly less than the global mean, with an increase of 0.60°C over the past century and a trend of 0.10°C per decade over the past 50 years (based on HadCRUT3v dataset; Brohan et al., 2006). The regional rate of increase is lower than the global rate because the region is dominated by ocean, and ocean temperatures are known to be increasing more slowly than land temperatures. Warming across the PCCSP region has not been uniform, with some datasets suggesting that data-sparse parts of the central equatorial Pacific have actually cooled over the past 50 years (Figure 3.2). It is unclear whether this cooling is real or an artefact of the analysis technique.

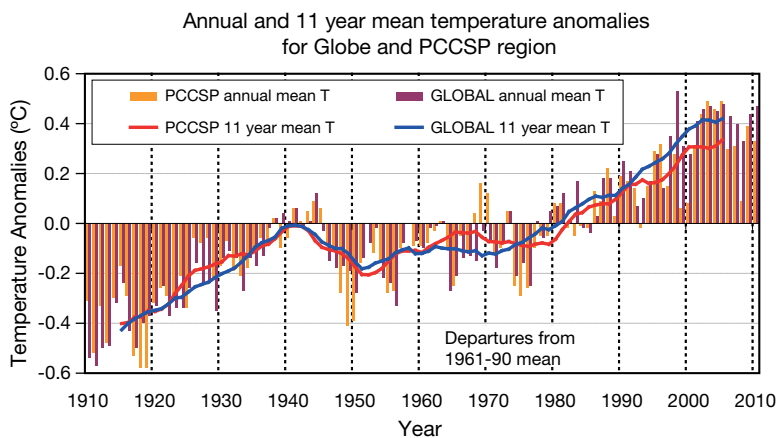


Figure 3.1: Annual mean surface air temperature anomalies from 1910–2010 for the globe and PCCSP region (120°E–210°E; 25°S–20°N), relative to the 1961–1990 mean. Solid lines indicate 11-year running means. (Based on HadCRUT3v dataset: Brohan et al., 2006).

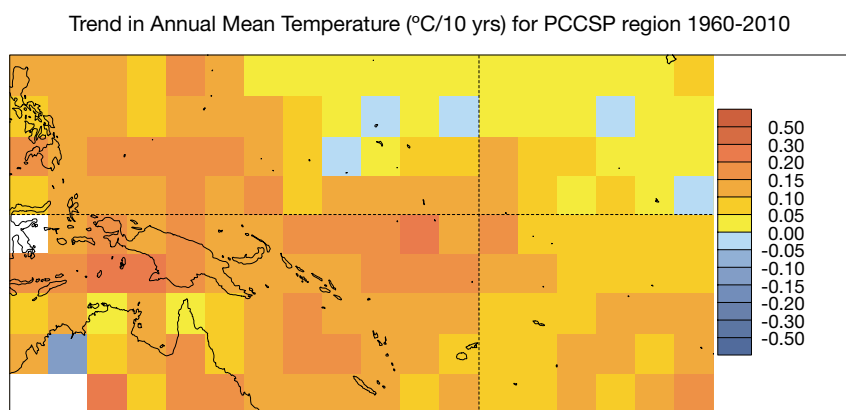


Figure 3.2: Trend in annual mean temperature (°C per decade) over 1960–2010, as determined by the HadCRUT3v global gridded temperature dataset (Brohan et al., 2006).

Box 3.1: Local Perceptions of a Changing Climate

There is general agreement amongst the communities of the Pacific Islands and East Timor that changes in weather and climate are occurring in their region. More change is believed to have occurred over the past decade than at any other time in human memory. Partner Country representatives have described local perceptions of climate change in their countries. These include:

- Shifts in seasonal patterns of rainfall and tropical cyclones.
- More frequent and extreme rainfall causing flooding and mudslides.
- More drought and fires.
- More hot days.
- Lower crop productivity.
- Spread of weeds, pest and diseases.
- More coral bleaching.
- More storm surges, coastal erosion and salt water contamination of freshwater springs and taro swamps.

Partner Country representatives have also reported that many Pacific Islanders believe that the impacts of climate change are being exacerbated by increased population and development, poor waste management and land degradation. Also, perceptions of vulnerability to climate change appear to differ between age, gender, religion, and socio-economic groups, with some studies

indicating that urban and wealthier people generally feel less vulnerable to the impacts of climate change (Wongbusarakum, 2009).

While some of the climate changes noted by Pacific Island people are consistent with anthropogenic global warming, human memory can be quite subjective regarding extreme weather and climate events. It is also difficult to scientifically confirm many of these changes due to a lack of sufficient data, highlighting the need for improved observation networks in the region. Detection and attribution of climate changes in the Pacific is further complicated by large changes in ENSO activity over the past century (Power and Smith, 2007). Consequently, it can be difficult to distinguish between natural interdecadal changes and those due to anthropogenic climate change, particularly at the local scale.

Some regional-scale changes in the Pacific have been partly attributed to human activities, e.g. weakening of the Walker Circulation (Power and Kociuba, 2011), and warming in the Pacific mean surface temperature (Stott et al., 2010). However, little research has been conducted to determine whether the changes perceived by people in the islands are real, and if so, to quantify the relative contributions from human and natural climate influences. The PCCSP represents a coordinated effort to begin to address these knowledge gaps.



Participants from PCCSP Partner Countries and other countries came together at a PCCSP workshop in June 2010 to discuss perceptions of climate change in their countries.

3.3 Climate of the Pacific over the Past 12 000 Years

3.3.1 Changes in Climate over the Holocene

The period from approximately 12 000 years ago to the present is known as the Holocene. It was preceded by a cold, glacial period that peaked around 21 000 years ago at the Last Glacial Maximum. Global average sea level at that time was around 120 m lower than that of today, due to the vast amounts of water that were locked up in expanded (Northern Hemisphere) ice sheets. The climate of the Holocene has been relatively warm and stable, allowing humans to develop agriculture and permanent settlements. People migrated across much of the Pacific Basin during this time (Nunn, 2007), with significant societal changes possibly linked to ENSO-driven environmental variability (Allen, 2006) and long-distance travel potentially assisted by reversals in the direction of the trade winds during El Niño events (Anderson et al., 2006).

There have been a number of large-scale changes in Pacific climate during the Holocene. Evidence from marine sediment records suggests that the Intertropical Convergence Zone (ITCZ) was located further north during the early Holocene (Haug et al., 2001), which may have led to drier and more saline conditions in the West Pacific Warm Pool (Stott et al., 2004). The ITCZ is thought to

have moved in response to shifts in seasonal solar radiation caused by changes in the Earth's orbit, with the changing position of the ITCZ driving variations in both the location and extent of the Indo-Pacific Warm Pool (Abram et al., 2009). The Asian monsoon is thought to have been stronger around 10 000 years ago and gradually weakened in response to the change in seasonal solar radiation (Wang et al., 2005). Lake level records from northern Australia suggest the Australian monsoon was stronger in the early Holocene (Wyrwoll and Miller, 2001). Stalagmites from Indonesia also suggest an increase in monsoon rainfall around 11 000 to 7000 years ago in association with rising global sea levels at this time (Griffiths et al., 2009).

During the past 10 000 years, ENSO variability is believed to have increased to its modern strength from a relatively weak level in the early Holocene (Tudhope et al., 2001). Proxy ENSO measures, such as charcoal evidence from northern Australia (Gagan et al., 2004); coral records (McGregor and Gagan, 2004); lake sediment records from Ecuador (Rodbell et al., 1999); and pollen records from northern Australia (Shulmeister and Lees, 1995), suggest that ENSO became stronger around 5000 years ago, with some evidence of a peak in activity around 2000 years ago (Woodroffe et al., 2003).

These changes would have had widespread impacts across the Pacific region, with likely increases in the frequency of extreme events such as droughts, floods, fires and tropical cyclones. Climate models suggest that the changes in ENSO activity during the Holocene were driven by changes in the seasonal incoming solar radiation associated with the precessional cycle of Earth's orbit (Brown et al., 2008; Phipps and Brown, 2010).

In New Zealand, the extent of Southern Alps ice has largely decreased over the Holocene (Schaefer et al., 2009), despite evidence that ice margin fluctuations and glacier re-advance episodes were numerous in the mid-to-late Holocene. Regional circulation dictates Southern Alps glacial activity and helps to modulate Southern Alps ice volume through changing precipitation and temperature regimes. Thus, ENSO, the Southern Annular Mode (Kidston et al., 2009; Ummenhofer et al., 2009), as well as the Interdecadal Pacific Oscillation, have probably combined to cause the glaciers to advance and retreat (Lorrey et al., 2010; 2011). Some of the past ice advances during the late Holocene occurred during Northern Hemisphere warm periods, indicating that Northern and Southern Hemisphere temperature changes have not always been in phase.

3.3.2 Changes in Climate over the Past 1000 Years

Variations in the global climate over the 1000-year period preceding the Industrial Revolution were driven by natural internal processes (e.g. ENSO) and natural external forcing factors (e.g. variations in solar output and stratospheric aerosols associated with major volcanic eruptions). Northern Hemisphere temperature reconstructions have identified a period of relatively warm temperatures (the Medieval Warm Period or Medieval Climate Anomaly) and a cooler period (the Little Ice Age). It is not clear if the Pacific region experienced the same climate variability (cf. Jansen et al., 2007).

The Medieval Climate Anomaly occurred around 1000–1300 A.D., and was associated with relatively high solar irradiance and low tropical volcanism. The warming found in reconstructions of Northern Hemisphere climate may not necessarily have been global. For example, a reconstruction using over 1000 different proxy records shows regions of both warming and cooling, with evidence for cool tropical eastern Pacific sea-surface temperatures

(Mann et al., 2009). An 1100 year tree ring record from New Zealand (Cook et al., 2002) implies the local climate was around 0.3 to 0.5°C warmer than the 20th century mean during the period 1000–1300 A.D., while a coral record from Palmyra, in the central Pacific, indicates local temperatures may have been cooler than present at the time of the Medieval Climate Anomaly (Cobb et al., 2003).

A synoptic palaeoclimate approach (Lorrey et al., 2007) was used to reconstruct atmospheric circulation patterns over New Zealand from a network of proxy records. While the late Holocene circulation has been variable (Lorrey et al., 2008), the frequency of blocking (stagnant) pressure patterns over the south-west Pacific increased during the Medieval Climate Anomaly (Lorrey et al., 2011), and has a different signature than the Northern Hemisphere.

The Northern Hemisphere Little Ice Age (ca. 1400–1850 A.D.) was associated with reduced solar irradiance and increased volcanic activity. Again, there is some evidence that the Little Ice Age was not experienced globally. For example, the Palmyra coral record (Cobb et al., 2003) suggests that the central tropical Pacific was relatively warm at that time.

The Palmyra coral record also provides information about changes in ENSO over the past 1100 years. The record suggests that during the mid-17th century ENSO events were stronger and more frequent than modern events, whereas during periods in the 12th and 14th centuries, ENSO activity was greatly reduced (Cobb et al., 2003). A tree ring reconstruction of ENSO over a six century period using North American tree ring records (D'Arrigo et al., 2005) found reduced ENSO amplitude in the late 17th to 18th centuries. Reconstructions based on multiple climate proxies have also shown that ENSO activity during the 20th century was unusual in that a high proportion of extreme and protracted El Niño and La Niña events occurred during this time (Gergis and Fowler 2009; McGregor et al., 2010). The Palmyra coral record implies that changes in ENSO over the last millennium may have arisen from natural internal variability (Cobb et al., 2003).

3.4 Major Features of Climate Variability

3.4.1 El Niño-Southern Oscillation and the Walker Circulation

ENSO is a major feature of interannual (year-to-year) climate variability in the Pacific. ENSO is a natural cycle of the climate system, characterised by distinct patterns of change in winds, surface pressure, surface and sub-surface ocean temperatures, precipitation, cloudiness and convection across the tropical Pacific. Consequently, ENSO has a powerful influence on the climate of the region. All PCCSP Partner Countries are affected by ENSO in some way, although the magnitude and timing of this influence varies between countries.

The ENSO cycle is irregular, and most of its variability has periods of two to seven years. The two extreme phases of the ENSO cycle are El Niño and La Niña. An El Niño is characterised by warming of waters in the central and eastern Pacific Ocean and cooling in a 'horse-shoe' pattern in the western Pacific Ocean, extending to the north-east and south-west (Figure 3.3a). This is known as the 'canonical' El Niño pattern and results in a reduction in the east to west sea-surface temperature gradient, which drives the Walker Circulation. Consequently, the surface trade winds forming the lower branch of the Walker Circulation weaken during El Niño. This reduces the east

to west sea-surface temperature difference, so the winds weaken further still. This completes a positive or self-reinforcing feedback loop. The existence of this feedback loop helps to make the tropical climate system unstable and this instability is partially responsible for the existence of ENSO. These changes in the atmosphere and ocean during El Niño also result in a displacement of the main area of convection from the western Pacific to east of the International Date Line. Opposite changes tend to occur during La Niña events, i.e. the central and eastern Pacific cools, trade winds strengthen and the main area of convection intensifies and moves further west than normal.

There are no universally agreed criteria to define El Niño or La Niña years. However, approximately one quarter of all years are usually defined as El Niño years, approximately one quarter as La Niña years and approximately one half as neutral years in which the anomalies described above are not apparent (Power and Smith, 2007).

El Niño and La Niña events usually begin to develop around May or June and last until the following March-May. However, while such events tend to follow a typical pattern of development, the strength and timing of each event is different, as is the exact pattern of sea-surface

temperature, wind and convection changes, and hence impacts.

A variation on the traditional canonical sea-surface temperature pattern of El Niño events involves the maximum warming occurring in the central tropical Pacific, rather than in the east (Figure 3.3b). This modified pattern is known as a 'central Pacific El Niño', or an 'El Niño Modoki' (Ashok and Yamagata, 2009). Whereas a canonical El Niño has anomalous ascending air over a large area covering the central to eastern Pacific overlying warmer sea-surface temperatures, during an El Niño Modoki the ascending branch occurs only in the central Pacific. El Niño Modoki is associated with distinct climate impacts compared to canonical El Niño events (Kumar et al., 2006; Wang and Hendon, 2007; Ashok et al., 2007; Weng et al., 2007; Taschetto and England, 2009). For example, in some seasons the impacts over regions such as New Zealand and the western coast of United States are opposite to those of a canonical El Niño.

ENSO is associated with large rainfall variations in many Partner Countries (Figure 3.4). Generally, countries east of about longitude 160°E and close to the equator experience above-average rainfall during an El Niño, while other countries, those west of longitude 160°E or more than about 10° from the equator, experience drier than

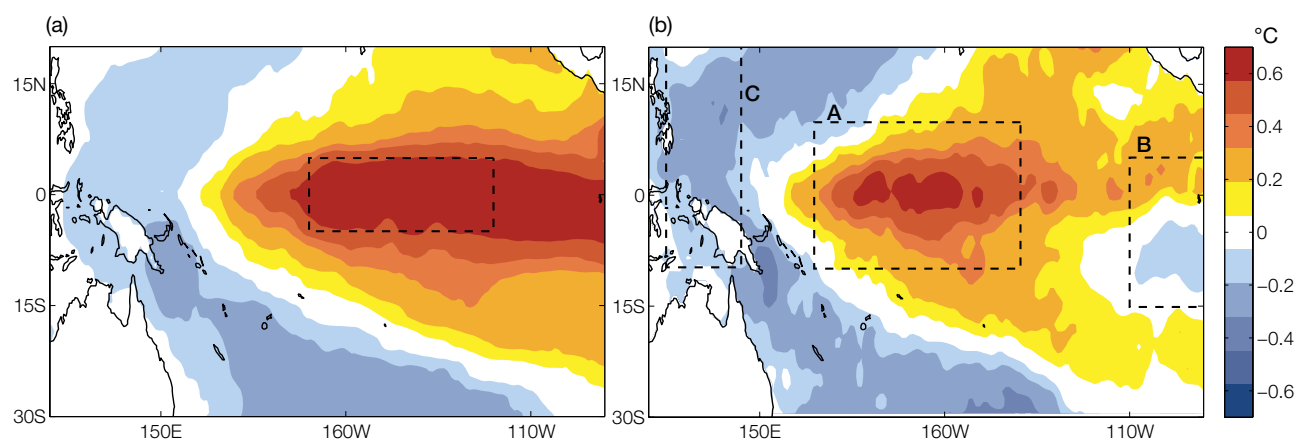


Figure 3.3: Sea-surface temperature anomalies (differences from average conditions) associated with (a) Canonical El Niño and (b) El Niño Modoki. (Source: Andrea Taschetto). Boxes show areas over which the (a) NINO 3.4 and (b) El Niño Modoki indices are calculated.

normal conditions. For most countries the average response in wet season rainfall is in the same direction for both canonical and El Niño Modoki events (Figure 3.4). However, in some places the response is weaker for El Niño Modoki, particularly for Partner Countries furthest to the south-east. Two exceptions are Nauru and Tarawa (Kirabati), due to these sites lying close to the centre of the largest sea-surface temperature anomalies that occur in Modoki events, and hence the greater response for El Niño Modoki.

ENSO is also associated with large year-to-year changes in the risks of drought, flood, tropical cyclones and coral bleaching throughout the region. Consequently, ENSO has significant impacts on agriculture, ecosystems, water resources, emergency management and disease (Philander, 1990, 2006; Power and Smith, 2007).

Numerous measures are used to monitor the status of ENSO. The Southern Oscillation Index (SOI) is an important example (Figure 3.5a). The SOI is calculated using the barometric pressure difference between Tahiti and Darwin, and is used as an indicator of the strength of the equatorial Walker Circulation and the Pacific trade winds (Power and Kociuba, 2010). A strong, persistently negative SOI is typical of El Niño conditions, while a strong and persistently positive SOI is indicative of La Niña.

Being a coupled ocean-atmosphere phenomenon, several measures of sea-surface temperature are used in conjunction with the SOI to monitor the oceanic component of ENSO. The Niño3.4 index (Figure 3.5b) measures the sea-surface temperature anomaly in the central and eastern Pacific between 170°W to 120°W and 5°S to 5°N (See Figure 3.3a). A strong, persistently positive Niño3.4 index (i.e. a warm central Pacific sea-surface temperature) corresponds to an El Niño event. Niño3.4 and the SOI are almost mirror images of each other, demonstrating the strong coupling between ocean and atmospheric changes.

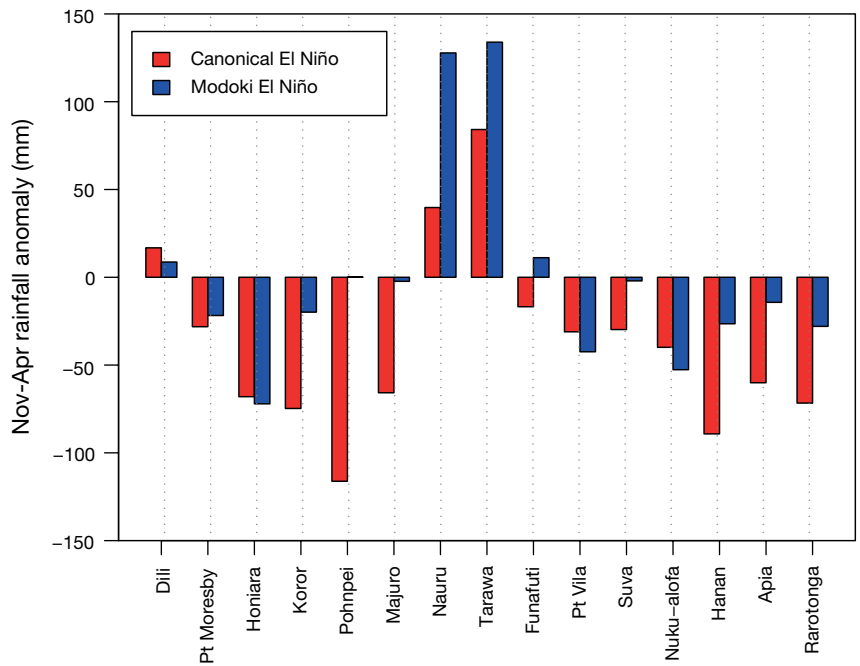


Figure 3.4: For sites in each Partner Country, differences between normal November to April rainfall and average rainfall during (red) Canonical El Niño events (years 1965, 1972, 1977, 1982, 1997, 2006, 2009) and (blue) Modoki El Niño events (years 1986, 1990, 1991, 1992, 1994, 2002, 2004).

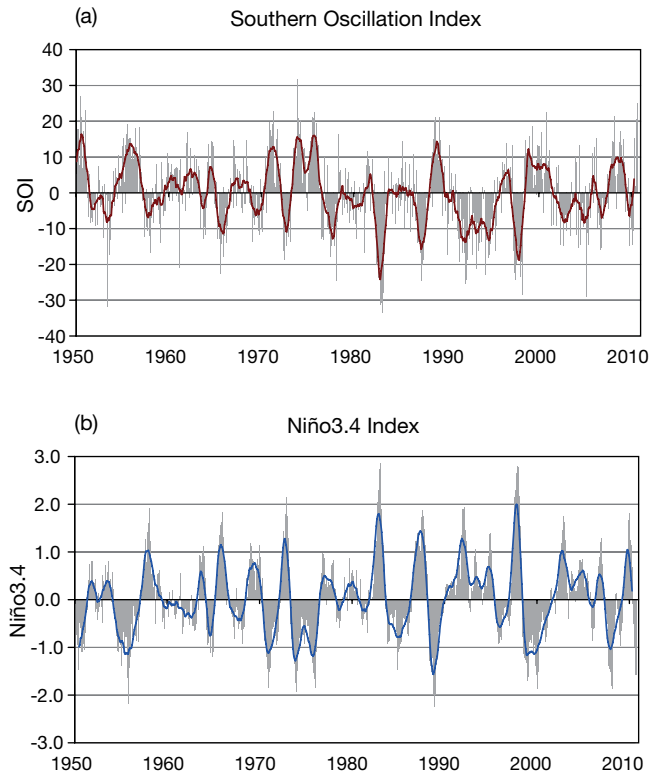


Figure 3.5: Monthly (a) SOI and (b) Niño3.4 values since 1950. Curves denote 12-month moving averages. (Source: SOI: <http://www.bom.gov.au/climate/current/soihtm1.shtml>; Niño3.4: <ftp.cpc.ncep.noaa.gov/wd52dg/data/indices/sstoi.indices>).

El Niño Modoki is measured by an El Niño Modoki Index (Ashok et al. 2007). Like the Niño3.4 index, it is calculated from average sea-surface temperature anomalies, but over three boxes: A: 165°E–140°W, 10°S–10°N; B: 110°W–70°W, 15°S–5°N; and C: 125°–145°E, 10°S–20°N, so that this index is equal to $A - 0.5*B - 0.5*C$ (See Figure 3.3b). Consequently, the index measures sea-surface temperature variations in the central equatorial Pacific Ocean against out-of-phase variations in the far eastern and far western Pacific Ocean.

Since the late 1970s the Modoki form of El Niño has become more frequent than the traditional El Niño (Ashok et al., 2007; Lee and McPhaden, 2010), with some scientists hypothesising that this might be related to anthropogenic global warming (Yeh et al., 2009). If so, this would suggest that this form of El Niño may become the dominant type in future.

In the past 100 years there have been interdecadal phases of strong and weak ENSO related to decadal variability from natural causes (Power et al. 2006; Collins et al. 2010). Along with the warming of the tropical Pacific in recent decades, there appears to have been a weakening of the Walker Circulation (Tanaka et al., 2004; Vecchi et al., 2006; Power and Smith, 2007; Collins et al., 2010; Power and Kociuba, 2010, in press). Theoretical arguments (Held and Soden, 2006) and model experiments (Vecchi et al., 2006) suggest that these changes are partly due to anthropogenic global warming. However, the changes can also be partially attributed to an increase in the frequency of El Niño events and a decrease in the frequency of La Niña events since 1975 (Fedorov and Philander, 2000; Power and Kociuba, 2010). Therefore the observed weakening of the Walker Circulation appears to have been driven both by global warming and random changes in the frequency of ENSO events.

Power and Kociuba (in press) examined the weakening of the Walker Circulation in response to internally generated natural variability and external climate forcing by examining simulations from global climate models with different natural and anthropogenic forcing. Internally generated natural variability is variability arising from instabilities in the atmosphere-ocean system such as ENSO and the Interdecadal Pacific Oscillation. External forcing is the term climate scientists use to cover forcing due to anthropogenic changes in greenhouse gases and aerosols, and forcing arising from natural changes in insolation (solar radiation) and volcanic activity. Most of the response to external forcing over the 20th century typically comes from the anthropogenic forcing. Power and Kociuba (in press) concluded that both internally generated natural variability and external forcing is needed to explain the observed 20th century weakening of the Walker Circulation, and that the magnitude of weakening caused by external forcing is similar to that of natural climate variability. This highlights the fact that trends in the region will typically have both an anthropogenic and a natural contribution.

3.4.2 Pacific Decadal Oscillation and Interdecadal Pacific Oscillation

Climate in and around the Pacific Ocean varies substantially on decadal time scales (Power et al., 1999a,b; Mann et al., 2000; Hasegawa and Hanawa, 2003; Kiem et al., 2003; Verdon et al., 2004; Power and Smith, 2007; Callaghan and Power, 2010). Much of this variability has been linked to natural ENSO-like patterns of variability operating at decadal and interdecadal time scales called the Pacific Decadal Oscillation (PDO) (Figure 3.16; Mantua et al., 1997) and the Interdecadal Pacific Oscillation (IPO, Power et al., 1999a).

The interdecadal variability in IPO and PDO indices are very similar (Power et al., 1999b). In fact the PDO can be regarded as the North Pacific manifestation of the Pacific-wide IPO (Folland et al., 2002). Countries influenced by the IPO are the same as the countries influenced by ENSO.

ENSO-like patterns of decadal variability can, in theory, arise from random changes in ENSO activity from decade to decade (Power and Colman, 2006). For example, a decade dominated by El Niño (e.g. a decade with two El Niño events and no La Niña events) will tend to have an El Niño-like sea-surface temperature pattern, whereas a decade dominated by La Niña (e.g. a decade with three La Niña events and only one El Niño event) will tend to have a La Niña-like decadal sea-surface temperature pattern.

While random changes in ENSO activity from decade to decade help explain the observed IPO and the PDO, such random changes alone cannot fully explain the spatial patterns and spectral properties of the IPO or the PDO (Power and Colman, 2006; Newman et al., 2003). For example, the unsmoothed PDO index has a lower frequency character than indices used to track ENSO (Newman et al., 2003), and the spatial pattern of the IPO has a broader meridional (north-south) structure near the equator in the eastern Pacific than ENSO in both observations and models (cf. Figure 3.3a and Figure 3.16, top; Power and Colman, 2006). The differences arise because the PDO and the IPO indices are influenced by slow oceanic processes (e.g. the storage of heat in the upper ocean and its evolution) and low-frequency oceanic Rossby waves (very large disturbances in ocean circulation that propagate across ocean basins).

Changes in the phase of the IPO have been linked to significant changes in climate regimes across the Pacific. For example, the rapid transition from a negative to a positive IPO phase during the mid-1970s was associated with a shift to an El Niño dominated period (Figure 3.6). The IPO switched to a negative phase around the year 2000, and the past decade has been dominated by La Niña.

The involvement of slow, natural oceanic processes can make some of the multi-year and decadal variability linked to the IPO and PDO more predictable than for ENSO (Power and Colman, 2006; McGregor et al., 2007, 2008, 2010; Mochizuki et al., 2010). However, the extent to which this translates into predictability of surface variables such as rainfall is unclear, though likely small (Power et al., 2006). This is the subject of ongoing research (Collins et al., 2010).

3.4.3 Intertropical Convergence Zone

The mean state of the ITCZ is described in Chapter 2. Seasonal and interannual variability in the position and intensity of the ITCZ can have significant impacts on low latitude Pacific nations due to its meridional narrowness and large rainfall gradients. As the mean seasonal shift of the ITCZ is relatively small, at only around 2° of latitude in the central Pacific, even small shifts in overall location can result in large impacts. As noted in Chapter 2, the PCCSP Partner Countries affected by the ITCZ are Palau, the Marshall Islands and the Federated States of Micronesia (see Table 2.4 and country reports in Volume 2 for further details).

Interannually, the ITCZ latitudinal location varies more in the December-February season than in June-August, with standard deviations of 1.5° and 0.6° of latitude respectively (Figure 3.7). Correlations with concurrent Niño3.4 temperatures are extremely high during both seasons (-0.94 and -0.85 respectively) indicating a strong link between ITCZ position and ENSO.

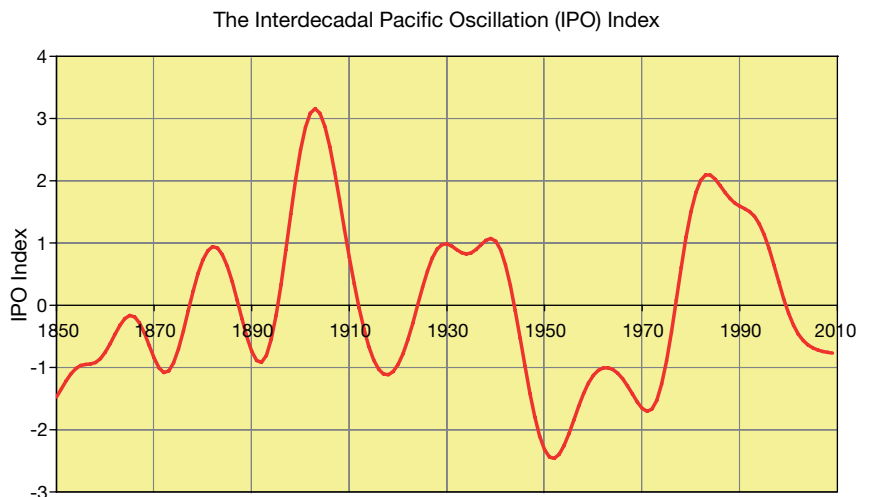


Figure 3.6: Time series of the Interdecadal Pacific Oscillation. (Data source: UKMO; Based on definition of Parker et al., 2007).

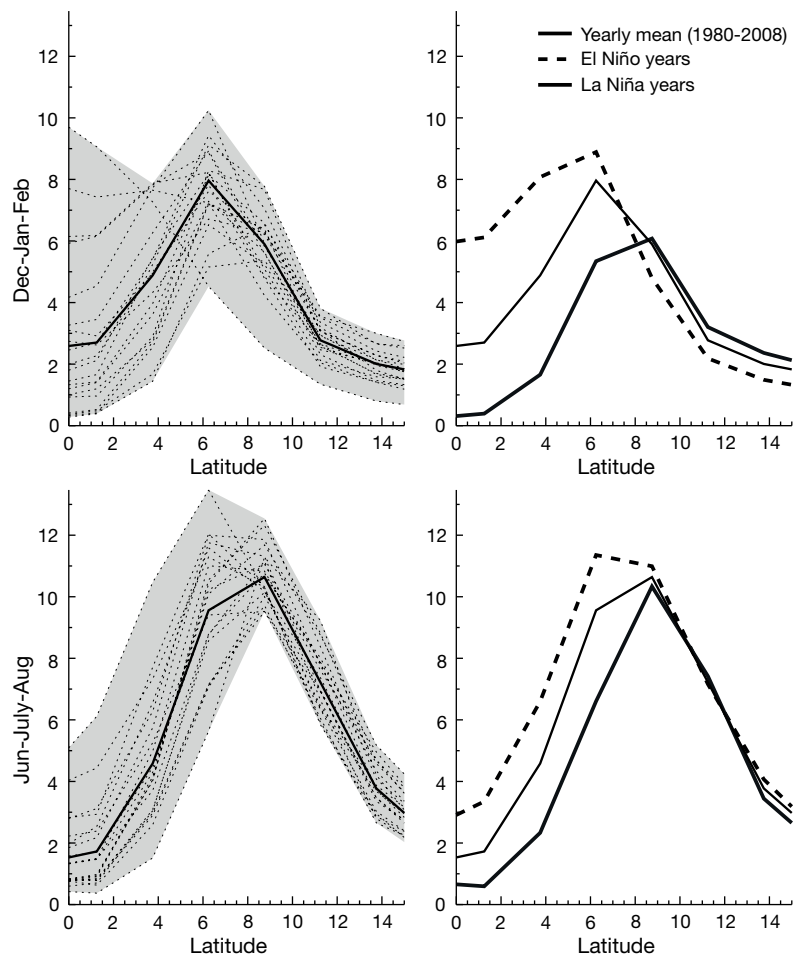


Figure 3.7: Observed meridional (north-south) variation of average precipitation for (top panels) December-February and (bottom panels) June-August for all years 1980–1999 (left panels) and for El Niño and La Niña years (right panels).

Over the 1979–1999 period the ITCZ, on average, was positioned around 3° closer to the equator during El Niño conditions than La Niña conditions; a difference larger than its mean seasonal variation. Rainfall amounts (again defined within the region 160°E–120°W, 0°–15°N) are also strongly correlated with Niño3.4 at around 0.74 in both the December–February and June–August seasons. A small downward trend in total rainfall is apparent over the 1979–1999 period for this region, and the trend is stronger in December–February than June–August.

3.4.4 Western Pacific Monsoon

The Western Pacific Monsoon is associated with a seasonal reversal of wind direction that brings heavy rainfall to the region north of Australia, extending from East Timor to the Solomon Islands. Variations in the timing, position, intensity, longevity and extent of the monsoon account for much of the rainfall variability in this region. As noted in Chapter 2, the PCCSP countries affected by the Western Pacific Monsoon are East Timor, Papua New Guinea and the Solomon Islands (see Table 2.4 and Volume 2 for further details).

The year-to-year variability in rainfall for December–February averaged over Southern Hemisphere box-1 (Figure 2.10) and June–August averaged over the Northern Hemisphere box (Figure 2.10) shows a downward trend during the 1980–1999 period (~90 mm per decade) for the Northern Hemisphere monsoon area, but only a weak downward trend for the Southern Hemisphere section (Figure 3.8). A strong correlation exists between rainfall in these regions and ENSO (shown in Figure 3.8 as seasonal mean Oceanic Niño3.4 Index, ONI), being -0.65 for the Northern Hemisphere box and -0.83 for Southern Hemisphere box-1.

The seasonal reversal of low-level winds is one measure of the regional extent of the monsoon (Wang, 2006). The extent of the westerly wind domain for each January during 1980–1999, as well the average extent for January during the same period, is shown in Figure 3.9. East Timor, Papua New Guinea and the Solomon Islands are within the monsoon region for all or most years. Vanuatu, Tuvalu and parts of Kiribati lie outside the average monsoon domain but nonetheless are affected by the monsoon during some years. In the Northern Hemisphere, Palau lies within the westerly domain during most years, while parts of the Federated States of Micronesia and Marshall Islands are only affected by the monsoon in some years.

Year-to-year variability in the extent of the monsoon-affected region is significant, especially on the eastern edge, where it varies by more than 5000 km between maximum and minimum extent. The north-south variability of the westerly wind domain is much less pronounced (Figure 3.9).

The time series of the position of the eastern edge of the westerly wind domain for December–February shows no long-term trend in the eastern extension of the monsoon domain during 1980–1999 for any of the three months (Figure 3.10). However, there is significant variability in the eastern edge within a single season, with the eastern edge moving on average by ~2500 km in every season. Between two different monsoon seasons, the variability in the position of the eastern edge of the monsoon domain is also large. The differences between the maximum and minimum extents are 2000 km for December, 1800 km for January and 2200 km for February. ENSO causes some of this variability. In fact, the two most extreme maximum eastern extents of the monsoon domain occurred during the strong El Niño years of 1983/84 and 1997/98 (Figure 3.10).

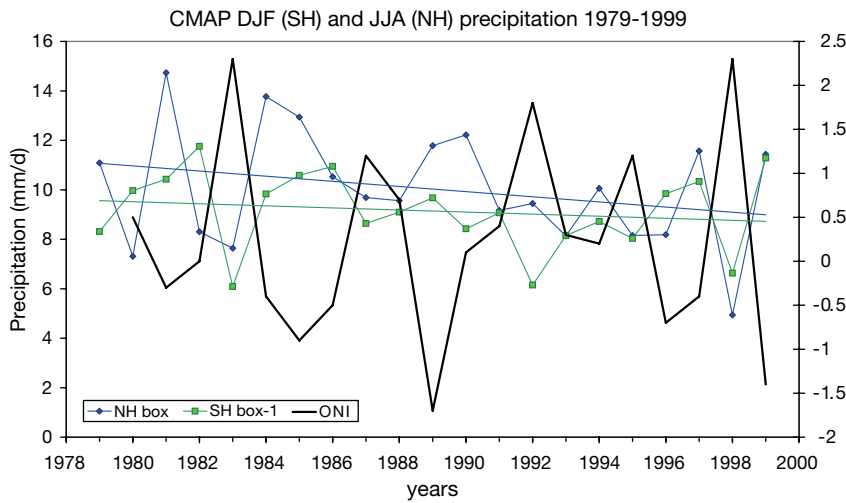


Figure 3.8: Seasonal mean rainfall (mm per day) averaged over Northern and Southern Hemisphere boxes (Northern Hemisphere box: 125–145°E; 5–10°N and Southern Hemisphere box-1: 120–150°E; 0–10°S, as shown in Figure 2.10). Seasonal averages are shown for June-August for the Northern Hemisphere box (blue) and for December-February for Southern Hemisphere box-1 (green) (Based on CMAP precipitation analysis). The Oceanic Niño3.4 Index (ONI) is shown in black.

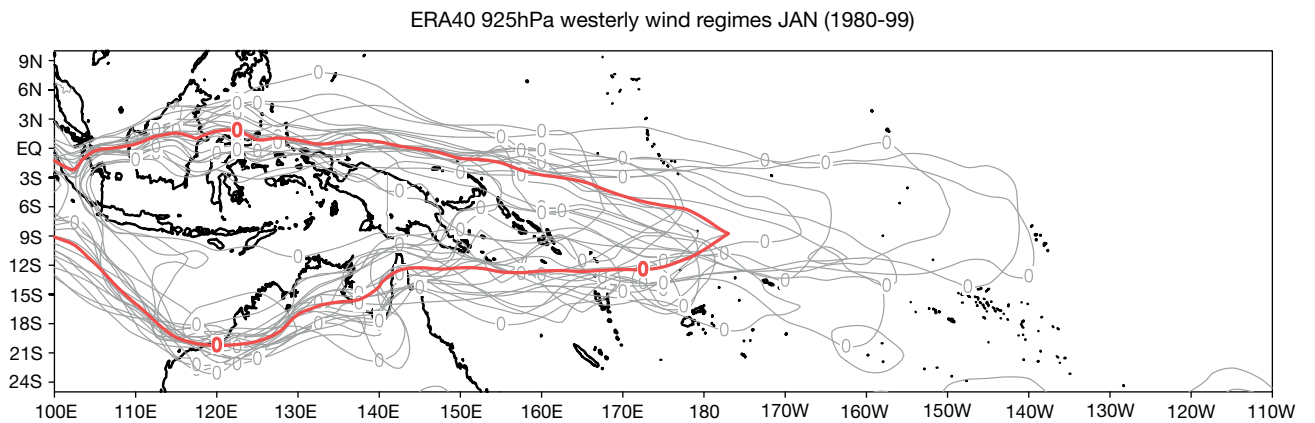


Figure 3.9: Interannual variability of the extent of the monsoon westerly wind domain during January. The extent for each individual January during 1980–1999 is shown in grey, with mean January extent during 1980–1999 shown in red. (Based on ERA-40 zonal winds at the 925 hPa level).

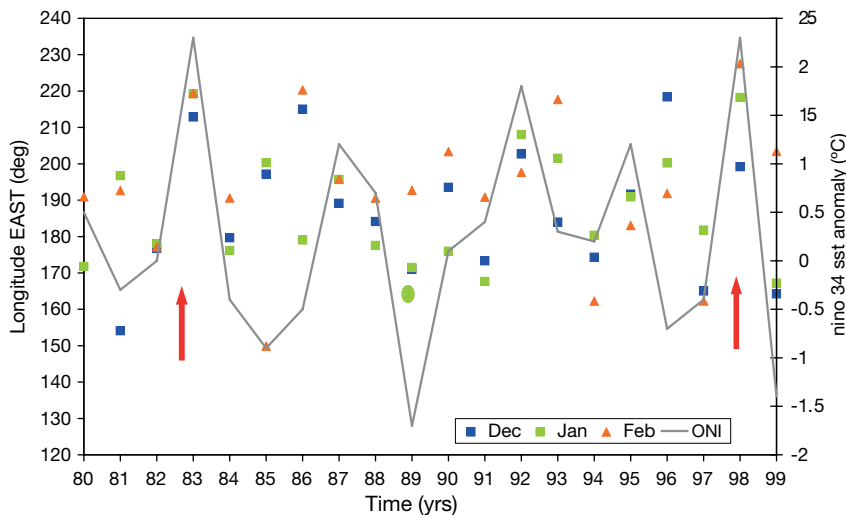


Figure 3.10: The most easterly position of the eastern edge of the monsoon westerly wind domain in December (blue), January (green) and February (orange) between 1980 and 1999. The December-February seasonal mean Oceanic Niño3.4 Index (ONI) is also shown (grey), with the major El Niños of 1983/84 and 1997/98 denoted by red arrows.

3.4.5 South Pacific Convergence Zone

The mean features of the SPCZ are described in Chapter 2. Fluctuations in the position of the SPCZ are a major cause of seasonal changes in rainfall, winds and tropical cyclone risk in many South Pacific Partner Countries. As noted in Chapter 2, the PCCSP countries affected by the SPCZ are the Cook Islands, Fiji, Kiribati, Nauru, Niue, Samoa, Solomon Islands, Tonga, Tuvalu and Vanuatu (Table 2.4 and Volume 2). The SPCZ Position Index is a measure of SPCZ location and is calculated as the normalised November-April difference at 9 am (local time) in mean sea-level pressure between Suva and Apia. It defines the latitude of the SPCZ between longitudes 180°W and 170°W (Folland et al., 2002).

The location of the SPCZ is closely linked with the phase of ENSO and the IPO/PDO (Folland et al., 2002). From the mid-1940s to the late 1970s, the SPCZ Position Index was more often negative than positive (Figure 3.11), indicating a tendency for the SPCZ to lie to the south-west of its mean position. Around 1980, the SPCZ Position Index underwent a rapid shift to more positive values, indicating a northward shift of the diagonal portion of the SPCZ, and a stronger sub-tropical high pressure belt (Griffiths et al., 2003). Since the late 1980s, the position of the SPCZ has oscillated around its long-term mean position.

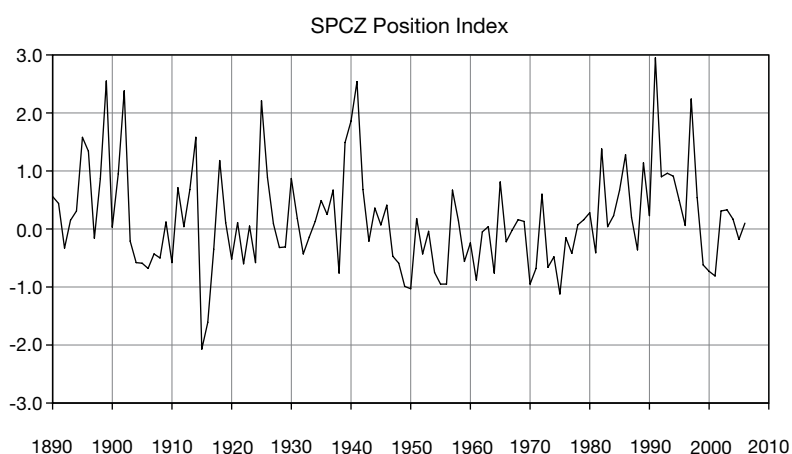


Figure 3.11: Index of the position of the South Pacific Convergence Zone during November-April (1891–2007). (Relative to the base period 1933–1992). Data courtesy of Jim Salinger.

3.4.6 Hadley Circulation

The Hadley Circulation is the dominant meridional circulation in the tropical atmosphere. Recent studies have suggested a poleward expansion of this circulation from the late 1970s using multiple datasets and methodologies (Birner, 2010; Hu and Fu, 2007; Siedel and Randel, 2007; Seidel et al., 2008). Many of these studies suggest that the observed expansion is larger in the Southern Hemisphere than the Northern Hemisphere. Lu et al. (2009) hypothesise that the expansion is a consequence of the radiative forcing associated with increased levels of greenhouse gases in the atmosphere and stratospheric ozone depletion. Changes to the intensity of the Hadley Circulation have been suggested (Mitas and Clement, 2005), although the magnitude of any such changes is unclear (Mitas and Clement, 2006).

As a whole, global climate models indicate a general meridional expansion and weakening of the Hadley Circulation in response to increased greenhouse gas forcing. This is hypothesised to be a result of increasing tropical static stability, which slows and weakens the overturning circulation. However, Johanson and Fu (2009) noted that the observed tropical expansion has proceeded more quickly than predicted by the models. They attribute this result to the role of stratospheric ozone depletion in driving the observed trends. The impacts of the expansion of the Hadley Circulation on Partner Countries remains poorly understood, but may turn out to be a significant consequence of global warming.

3.4.7 Southern Annular Mode

In the Southern Hemisphere extra-tropics the atmospheric circulation is dominated by strong mid-latitude westerly winds. There are important variations in the strength and the position of these winds: they tend to oscillate between being stronger and more poleward, or weaker and more equatorward. This characteristic pattern of variability in the westerlies is known as the Southern Annular Mode (SAM; Thompson and Wallace, 2000). While this feature primarily affects higher latitude land masses (Gillett et al., 2006; Hendon et al., 2007) and oceans (Sen Gupta and England, 2006), it may directly impact southern parts of the PCCSP region (south of about 20°S) via changes in the atmospheric circulation. The SAM may also indirectly affect the wave climate of the region by modifying the large swell waves generated by storm activity in the Southern Ocean that can travel into the tropical Pacific and affect wave height (Hemer et al., 2008).

The SAM can be represented by an index based on the difference in pressure between 40°S and 65°S (Marshall, 2003). A positive SAM is associated with both a strengthening and poleward shift of the westerlies, and an intensification of storm activity. As a result, the sub-tropical high pressure systems that migrate from west to east at around latitude 30° (Section 2.3.1) move away from the equator as well, affecting local weather conditions. The reverse occurs during the negative phase of the SAM: the band of westerly winds are weaker and situated closer to the equator, with weaker storm activity and cold fronts located closer to the sub-tropics. The SAM may therefore affect the climate of all PCCSP countries in the South Pacific sub-tropics.

Since the mid-1960s the SAM has undergone a robust change towards its more positive phase (Thompson and Wallace, 2000; Marshall, 2003). Observational and modelling studies have demonstrated that these trends are consistent with a combination of recent stratospheric ozone depletion and enhanced greenhouse gas forcing (Fyfe et al., 1999; Thompson and Solomon, 2002; Gillett and Thompson, 2003; Cai and Cowan, 2007). The increase in storm intensity associated with the positive phase of the SAM could be expected to increase swell magnitudes in southern parts of the South Pacific (Hemer et al., 2008), but the southward shift in the location of the storm tracks may act to counteract the effect of this increased intensity.

Long-term changes in the SAM can also drive changes in the sub-tropical ocean circulation. Observational evidence suggests an increase in the strength of the South Pacific sub-tropical gyre since 1993, and an associated warming of the Tasman Sea (Roemmich et al., 2007).

3.4.8 Indian Ocean Dipole

The Indian Ocean Dipole (IOD) is a pattern of interannual variability in the tropical Indian Ocean basin that involves ocean-atmosphere interactions in the east-west direction (Saji et al., 1999; Webster et al., 1999; Yu and Rienecker 1999). A positive IOD event refers to a pattern of sea-surface temperature variability in which ocean-surface conditions are cool relative to the long-term average in the east equatorial Indian Ocean and warm in the west. A negative IOD event has the opposite pattern. Similar to ENSO, the IOD is associated with a positive

feedback process involving winds that result in a shallower thermocline, influencing zonal sea-surface temperature gradients, which in turn reinforce the winds. An IOD event usually starts to develop in June and peaks in September-November.

The IOD influences climate both locally and in remote regions. For example, a positive IOD event is associated with droughts in East Asia (Guan and Yamagata, 2003), south-east Australia (Cai et al., 2005; Meyers et al., 2007; Cai et al., 2009a), Indonesia and East Timor (D'Arrigo and Smerdon, 2008), and flooding in parts of India and East Africa (short rains; Black et al., 2003). It also affects the Indian and Australian monsoons (Ashok et al., 2001). However, the IOD is a much weaker source of climate variability for the Pacific region than ENSO and its independence from ENSO remains a subject of scientific debate (Dommenges, 2010). Its influence on PCCSP Partner Countries other than East Timor is uncertain. Some evidence suggests a trend towards an increasing frequency of positive IOD events and decreasing frequency of negative IOD events (Cai et al., 2009b).

3.5 Variability and Change in the Atmosphere

3.5.1 Temperature

Previous studies of temperature trends in the Pacific used data recorded by the respective national meteorological services to show that temperatures generally increased throughout the Pacific Islands during the 20th century (Salinger, 1995; Folland et al., 2003). However, these trends have not been spatially uniform. Changes in temperature extremes have tended to follow those of mean temperatures, with most stations showing an increase in the occurrence of hot days and warm nights, and a decline in the number of milder days and cooler nights over the last four decades of the 20th century (Manton et al., 2001; Griffiths et al., 2005).

Long-term temperature trends in the Pacific have been updated here by the PCCSP through collaboration with the national meteorological services in Partner Countries. These temperature records have undergone homogeneity assessment and adjustment (Wang, 2009) where appropriate to produce reliable analyses of temperature trends. Unfortunately only limited data could be sourced for East Timor and Nauru, preventing the calculation of trends for these Partner Countries.

The updated PCCSP region temperature records show clear and consistent warming over the past 50 years (Figure 3.12), with most stations recording trends around +0.08–0.20°C per decade over this time. The strongest warming is found in Papua New Guinea and French Polynesia. Trends in maximum and minimum temperatures are generally similar to those of mean temperature at most stations, apart from in Fiji, Tonga and Niue where there is a tendency for greater warming in the daytime. The amount of warming in the wet and dry seasons is also similar at most stations. The magnitude of background warming in PCCSP region temperature records over the past half-century is consistent with that expected from human-induced global warming.

3.5.2 Rainfall

Much of the variability in Pacific Island rainfall records is closely linked to ENSO and the IPO (Salinger et al., 2001), and directly attributable to shifts in the SPCZ or ITCZ (McCarthy et al., 2001; Folland et al., 2002). The effects of SPCZ movement on mean rainfall regimes in much of the South Pacific have been large in the past century. Increases of mean annual rainfall of 30% or more occurred north-east of the SPCZ between the most recent positive phase of the IPO (1978–1998), and the previous negative phase (1946–1977; Salinger et al., 2001). Decreases in mean annual rainfall to the south-west of the SPCZ were smaller, but both changes were consistent with a movement in the mean location of the SPCZ to the north-east.

Previous studies of rainfall trends show that over the 1961–2000 period, locations to the north-east of the SPCZ became wetter, with the largest trends occurring in the eastern Pacific Ocean (east of 160°W), while locations to the south-west of the SPCZ became drier (Griffiths et al., 2003). Trends in the frequency of rain days were generally similar to those of total annual rainfall,

with more (less) rain days typically associated with more (less) total rainfall (Manton et al., 2001; Griffiths et al., 2003). Overall, rainfall changes determined by previous studies are consistent with the SPCZ having moved north-east over the 1960–2000 period (Figure 3.11).

Changes in extreme rainfall in the Pacific have been analysed by defining indices to measure extreme frequency, intensity, proportion of total rain and dry spell length (Manton et al., 2001; Griffiths et al., 2003). Trends in these indices have tended to mirror those of total rainfall. Changes in extreme rainfall during the last four decades of the 20th century are thus also consistent with the SPCZ having moved north-east.

Due to the paucity of rainfall station data in the Pacific, many of the global gridded precipitation datasets show large voids in the region. Consequently, rainfall trends are best analysed using station data. Rainfall series from land based stations have been updated and adjusted for homogeneity where appropriate, in collaboration with national meteorological services and other agencies in Pacific Island countries and East Timor.

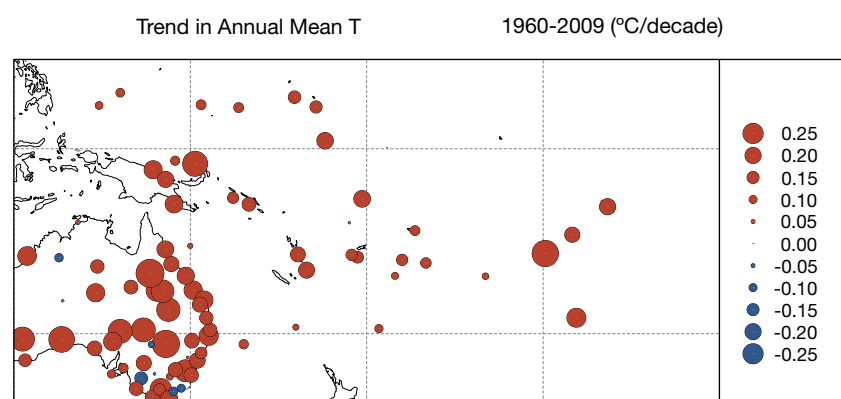


Figure 3.12: Sign and magnitude of trends in annual mean temperatures at Pacific Island meteorological stations for 1960–2009. Australian stations included for comparison.

The updated rainfall series clearly show the large interannual variability experienced in the tropical Pacific. This variability is large compared with the magnitude of long-term rainfall trends, making them less spatially coherent than those for temperature. Trends in total annual rainfall for the longest available rainfall records, indicate a general increase in rainfall totals north-east of the SPCZ over the past 50 years (Figure 3.13a), with mainly declines to the south-west of the SPCZ, and north of the ITCZ just west of the International Date Line. This pattern of change is generally reflected in both wet and dry seasons. However, the pattern of trends has changed markedly in the south-west Pacific over the past two decades (Figure 3.13b), consistent with a shift of the SPCZ back to its climatological position since 1990 (Figure 3.11).

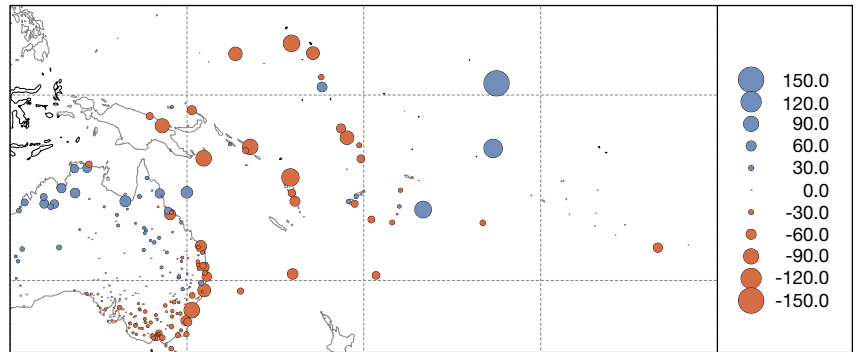
Unlike changes in temperature, which are dominated by background global warming, the lack of a sustained trend in rainfall suggests that Pacific rainfall patterns continue to be strongly influenced by natural climate variability.

3.5.3 Tropical Cyclones

ENSO plays a role in modifying tropical cyclone risk throughout the tropical Pacific. When the western equatorial Pacific warms relative to the eastern equatorial Pacific during the La Niña phase, cyclones occur with greater frequency in the western Pacific, close to Australia (Figure 3.14). Conversely, during the El Niño phase, when the western equatorial Pacific is anomalously cool, the region of greatest cyclone occurrence is found further east.

The analysis of trends in the historical tropical cyclone record has been difficult. Some studies (Webster et al., 2005) describe trends towards more intense tropical cyclones in parts of the world, e.g. the North

(a) Trend in Annual Rainfall 1960-2010 (mm/decade)



(b) Trend in Annual Rainfall 1990-2010 (mm/decade)

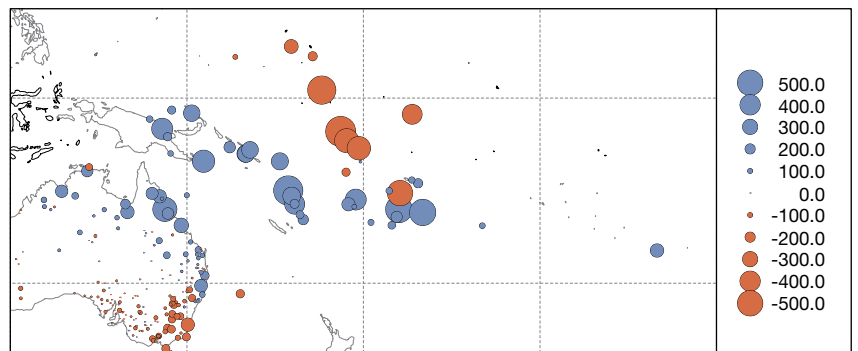


Figure 3.13: Trends in annual total rainfall at Pacific meteorological stations for (a) 1960–2010 and (b) 1990–2010. Note different scales on plots. Refer to Volume 2 of this report for individual station time series.

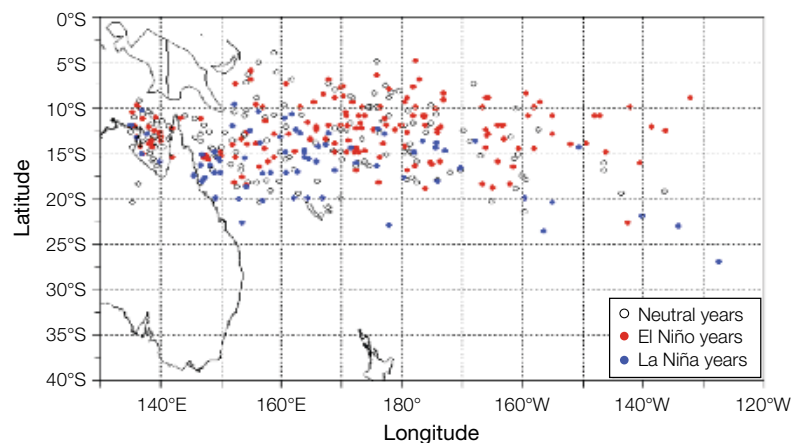


Figure 3.14: Locations where tropical cyclones formed over the South Pacific Ocean in neutral (grey), El Niño (red) and La Niña (blue) years during 1969–2006. Genesis location is defined as the point where tropical cyclone central pressure is estimated to have dropped to 1000 hPa or lower (Source: Kuleshov et al., 2009).

Atlantic Ocean and the north-west Pacific region, while other studies (Chan, 2006; Landsea et al., 2006; Curry et al., 2006) dispute these findings on the basis that changes in observation technology and analysis techniques over time have created spurious trends in the observational record. Using three different tropical cyclone archives, Song et al. (2010) found contrary trends in the proportion of intense tropical cyclones in the western North Pacific over the past few decades. They concluded that different algorithms used in determining tropical cyclone intensity in each of the archives may account for these discrepancies.

A rigorous analysis of the South Pacific tropical cyclone archive indicates no significant trends in the total number of tropical cyclones over 1981–2007, nor in the overall number of intense tropical cyclones in the South Pacific Ocean (Figure 3.15; Kuleshov et al., 2010). However, this is a very short period over which to examine trends in

extreme events. As complete records of estimated tropical cyclone intensity are only available from 1981, studies of tropical cyclone numbers are limited to this time. It is important to note that the absence of overall trends for the South Pacific does not discount the possibility of local trends. However, as shown in the country summaries in Volume 2 of this publication, tropical cyclone numbers show large interannual variability at the local level, making it virtually impossible to identify long-term trends at local and national scales.

An analysis of published case studies, seasonal summaries, newspaper archives and historical society records dating back to the late 19th century (Callaghan and Power, 2010) indicates that the frequency of severe tropical cyclones making landfall over north-eastern Australia varies substantially on interannual, decadal and longer time scales. The sign and magnitude of trends calculated over 30-year periods varies greatly for these

Australian landfalling tropical cyclones, highlighting the need for caution in making inferences about trends based on short time spans, such as the satellite era (from the 1970s). While the number of landfalls fell over the period 1872–2010, the declining trend is only significant at the 90% level. Callaghan and Power (2010) also concluded that prudent planning should reflect the possibility of a rapid return to the much higher landfall rates seen earlier in the record.

3.5.4 Other Variables

Studies of changes in atmospheric variables other than temperature, rainfall and tropical cyclones are rare for the Pacific region, reflecting a lack of available data. One study showed that trends in sunshine hours and 9 am cloud amount in the Pacific region over the 1951–1990 period were weak and mixed throughout the region (Salinger et al., 2001).

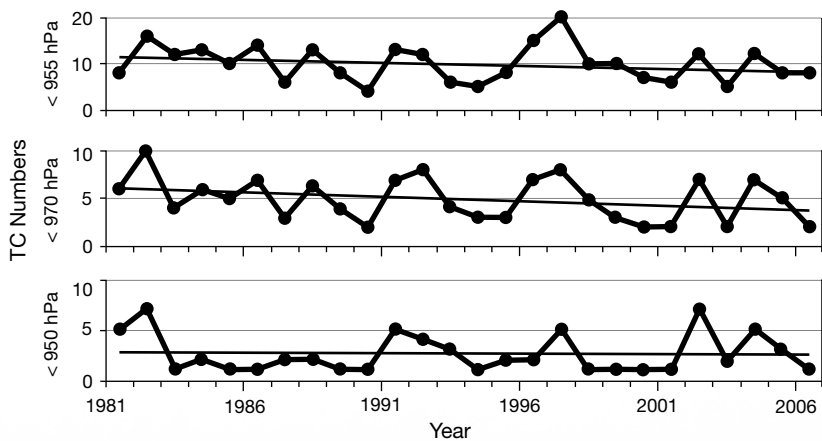


Figure 3.15: Number of tropical cyclones per year over the South Pacific Ocean for the 1981–2007 period. Series represent numbers of tropical cyclones with minimum central pressure of 995 hPa or lower (top), 970 hPa or lower (middle) and 950 hPa or lower (bottom). (Source: Kuleshov et al., 2010).

3.6 Variability and Change in the Ocean

The ocean dominates the PCCSP region. Changes to ocean characteristics affect marine biological systems and, in turn, the vital regional fisheries. In addition, interactions between the ocean and atmosphere mean that changes in the atmosphere, and on the islands, are strongly influenced by the state of the ocean. For example, ENSO owes its existence to oscillations in the location of warm water in the western Pacific Ocean and the resulting feedback this causes in the atmosphere. On longer time scales, the predominance of ocean in the region means that the regional mean temperature has risen more slowly than the global mean over recent decades.

3.6.1 Sea-Surface Temperature and Salinity

At tropical latitudes, year-to-year variability is often larger than seasonal changes. The predominant pattern of interannual change in the ocean is associated with ENSO (Section 3.4.1). On longer time scales, the PDO/IPO (Section 3.4.2) are associated with important modulations in large-scale ocean temperature and circulation. As already discussed, the pattern of sea-surface temperature changes associated with the PDO (Figure 3.16, top) are similar to those during ENSO, although the pattern extends further away from the equator, and the oscillation between positive and negative phases can take decades, rather than a few seasons (Figure 3.16, bottom). The existence of natural variability with such long time scales complicates the attribution of trends in ocean temperatures by making it difficult to determine what is related to global warming and what is simply part of natural variability.

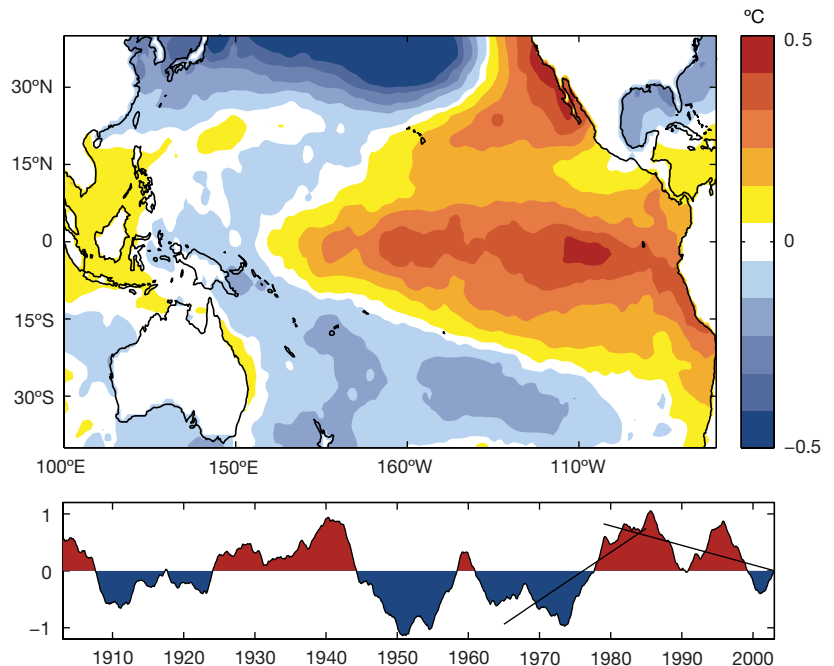


Figure 3.16: (Top) Pattern of sea-surface temperature associated with a positive, warm phase (+1 standard deviation) Pacific Decadal Oscillation (PDO) event. (Bottom) Time series of the PDO (red: warm phase, blue: cold phase) with linear trends for the periods 1979–2008 and 1965–1985 superimposed (Data source: HadISST).

There are a number of different sea-surface temperature datasets that, while based on essentially the same set of observations, use different interpolation methods to account for missing data. Based on two of these datasets the 50-year trends reveal broad-scale warming in most areas (Figure 3.17). However, as a consequence of data scarcity across parts of the tropical Pacific region, there is disagreement in the sign of the trends in some locations. This is further discussed in Deser et al. (2010). Cravatte et al. (2009) found that most datasets show a consistent long-term warming in the western Pacific, up to 0.75°C over 1959–2008, while there is less consistency in the central and eastern equatorial Pacific.

A further difficulty with trend calculation is related to the 'noise' associated with natural variability on interdecadal and longer time scales. The pattern of change varies considerably, depending on the time period over which the trend is computed. For example, over

the 1979–2008 period, sea-surface temperatures show broad cooling in the eastern equatorial Pacific and warming in the west, while over 1965–1985 this pattern is essentially reversed (irrespective of the dataset used). While warming in the mean Pacific surface temperature has been partially attributed to human-induced global warming (Stott et al., 2010), part of the slowly varying changes evident can also be attributed to natural variability, e.g. IPO/PDO (see trend lines on Figure 3.16, bottom). Large swings in the IPO/PDO indices are often termed regime shifts in the climate dynamics (Mantua and Hare, 2002) and are associated with major biological and climate shifts. The extent to which these shifts are actually predictable on decadal time scales is the subject of ongoing research (Newman, 2003; Power et al., 2006; Power and Colman, 2006; Collins et al., 2010) and will be a major focus for the next IPCC Assessment Report (Taylor et al., 2009).

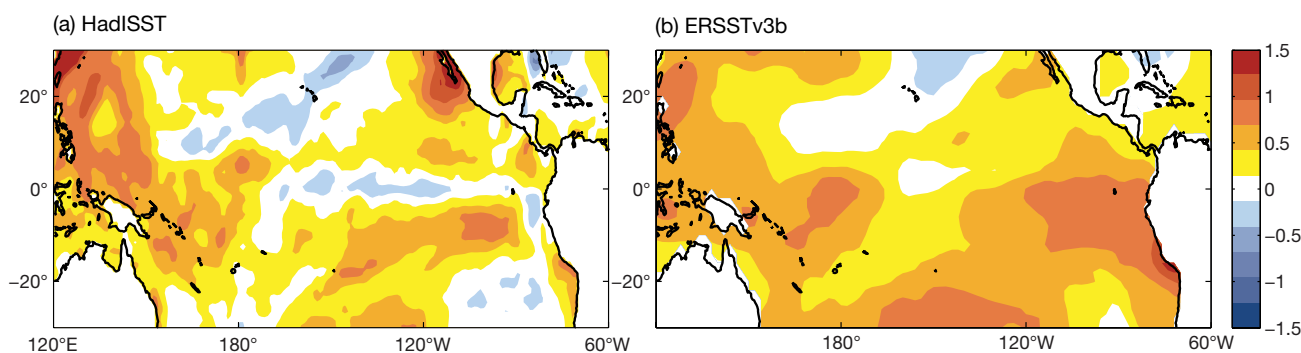


Figure 3.17: Comparison of linear trend in sea-surface temperature ($^{\circ}\text{C}$ per 50 years) over 1959–2008 for two observational datasets. (a) HadISST, <http://badc.nerc.ac.uk/data/hadisst/>; (b) ERSSTv3b, <ftp.eclipse.ncdc.noaa.gov>.

Salinity measurements in the equatorial Pacific Ocean are much sparser than temperature measurements, making the identification of trends even more difficult. Nevertheless, a significant freshening seems to have occurred over the western tropical Pacific, extending eastward under the low salinity ITCZ and SPCZ regions (Figure 3.18; Durack and Wijffels, 2010). Conversely, regions to the east have generally become saltier. These observations suggest that there has been an increase in rainfall relative to evaporation in the western tropical Pacific and an increase in evaporation relative to rainfall in the east, i.e. an intensification of the hydrological cycle across the equatorial Pacific over recent decades.

As the west equatorial Pacific Warm Pool has warmed and freshened during recent decades, the extent of the Warm Pool has grown considerably. For example, the area of water with temperatures exceeding 29.5°C has increased by 400–600% (Cravatte et al., 2009).

3.6.2 Sub-Surface Temperature and Salinity

To examine changes in temperatures below the ocean surface, a new observational dataset based on over 2.6 million historical temperature profiles has been developed. The analysis explicitly accounts for the effects of global and

regional natural climate fluctuations (including ENSO, PDO, SAM and the North Atlantic Oscillation) and climate drivers (including increased greenhouse gases, stratospheric volcanic aerosols and total solar irradiance). A new salinity dataset has also been developed using over 1.6 million profiles of salinity, potential temperature and neutral density from historical archives and the international Argo project (Durack and Wijffels, 2010). The dataset extends from 1950–2008, which minimises bias in the trend calculation associated with ENSO.

A distinctive pattern of intensified surface warming and sub-surface cooling centred near a depth of 200 m is evident for the 1950–2008 period (Figure 3.19). The sub-surface

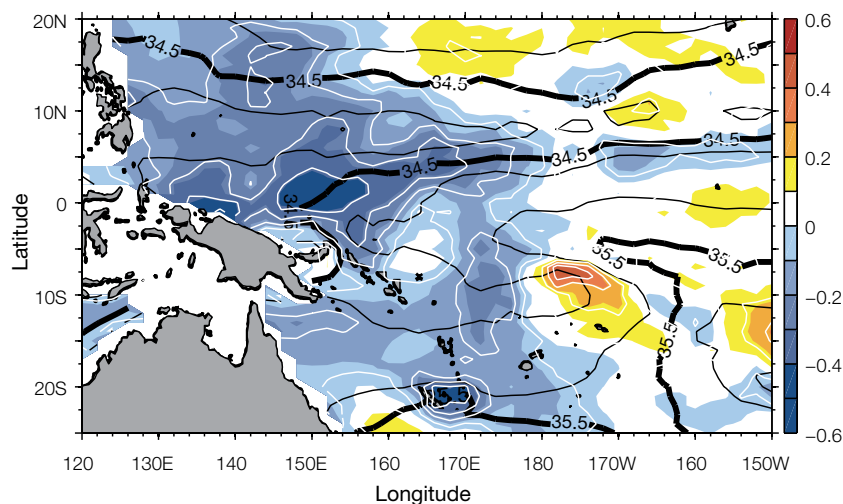


Figure 3.18: Surface salinity trend (psu per 50 years) in the tropical Pacific Ocean based on data from 1950–2008 (with 0.125 psu per 50 years contour interval shown in white). Mean salinity is overlaid in black (contour interval 0.25, and thick contours every 0.5). (Source: Durack and Wijffels, 2010).

cooling is probably a result of changes in the overlying wind field that causes the thermocline to be shallower (Han et al., 2006). A similar pattern of change, albeit with weaker magnitude, is evident in many of the climate model simulations of historical change (Chapter 4). As this change in the climate model simulations is due to increased concentrations of atmospheric greenhouse gases (and not natural climate variability) it suggests that the observed pattern is a result of human-induced changes, rather than natural variability.

The linear trend in sub-surface ocean temperature is larger than anything that can be explained by solar and volcanic activity, or by the natural fluctuations associated with the North Atlantic Oscillation, SAM and PDO. Only ENSO could potentially result in signals of this magnitude, but this is only true within the tropics. The temperature trend is statistically significant over most of the Pacific Ocean, however, and so cannot be fully explained without human-induced warming.

Large, significant and spatially coherent multi-decadal trends in salinity, down to a depth of 2000 m, are also evident in the Pacific. Much of the sub-surface change is consistent with an upward movement of the thermocline. Intensified surface warming and freshening both act to reduce upper ocean density, thus

intensifying ocean stratification and suppressing vertical mixing, making it harder to bring sub-surface nutrients into the upper ocean (where they are used in primary production).

3.6.3 Sea Level, Waves and Surges

3.6.3.1 Past Sea-Level Change

Information on how sea level has changed through Earth's history provides valuable insight as to what sea levels might be possible in the future and what rates of change are feasible. The last time the Earth was essentially free of major ice sheets was about 35 million years ago. At that time the atmospheric carbon dioxide concentration was 1250 ± 250 ppm, the Earth was warmer as a result of larger atmospheric greenhouse gas concentration and sea level was about 70 m above present-day values (Alley et al., 2005). As greenhouse gas concentrations fell after this period, the Earth cooled and the major ice sheets formed, first in the Antarctic and then later in the Northern Hemisphere. Over the glacial cycles of the past 500 000 years, sea level has vacillated by more than 100 m as the great ice sheets, particularly those of northern Europe and North America, waxed and waned (Rohling et al., 2009).

During the last interglacial period (about 125 000 years ago) temperatures were about 3°C warmer than today due to a natural variation in the Earth's orbital parameters. These temperatures are similar to what could be expected late in the 21st century if greenhouse gas emissions continue to rise at the rate of the past decade. Analysis of geological records indicates a 95% probability that global sea level peaked at least 6.6 m higher than today but was unlikely (33% probability) to have exceeded 9.4 m (Kopp et al., 2009). About the time when global sea level was close to its current level or higher, the millennial average rate of global sea-level rise is very likely to have exceeded 5.6 m per millennium but is unlikely to have exceeded 9.2 m per millennium (Kopp et al., 2009). A record in the Red Sea indicates higher rates of 1.6 ± 0.8 m per century (Rohling et al., 2008). Higher rates of rise may have occurred over shorter periods but it is not yet possible to definitively quantify these from the available data. It may take some time for the ice sheet contributions to sea-level rise to accelerate to these rates but the palaeo-data highlight the long-term vulnerability of ice sheets to sustained global warming.

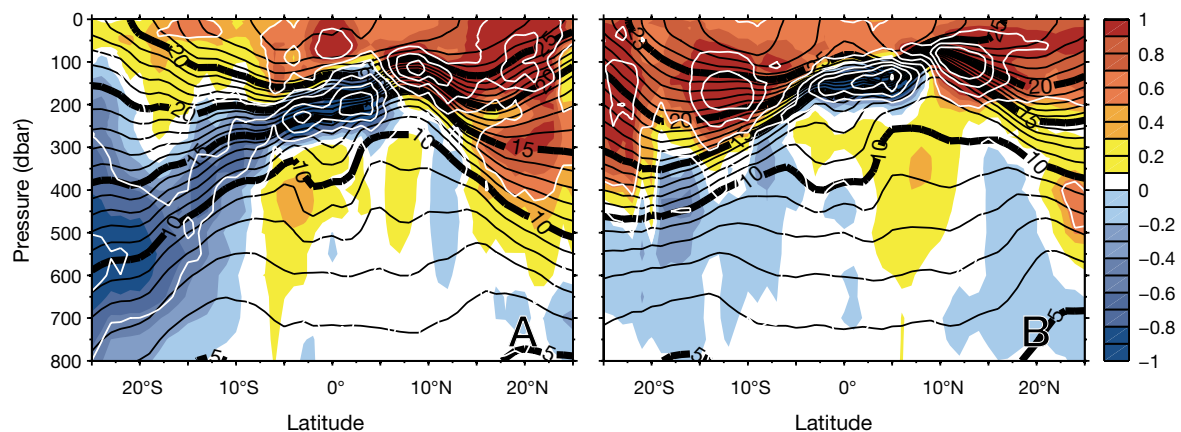


Figure 3.19: Temperature trend ($^{\circ}\text{C}$ per 50 years) in the tropical Pacific Ocean based on the years 1950–2008. Mean temperature is overlaid in black (contour interval 1°C , and thick contours every 5°C), and temperature changes are contoured in white (contour interval 0.5°C from -2°C to $+2^{\circ}\text{C}$). Vertical meridional sections at (A) 160°E and (B) 160°W are shown (Source: Durack and Wijffels, 2010).

From the last interglacial period to the last glacial maximum about 20 000 years ago, sea level fell by over 120 m as major ice sheets formed over northern America, Europe and Asia, and the Antarctic ice sheet grew (Lambeck and Chappell, 2001). From about 20 000 years ago until about 7 000 years ago, sea level rose rapidly at average rates of about 1 m per century for many millennia. Recent estimates (Stanford et al., 2011) suggest the highest rates during this period were probably less than 2.6 m per century (99% confidence limits), although Clark et al. (2002) have estimated rates of as large as 4 m per century. However, these conditions are probably not analogous to the 21st century sea-level change because of the much larger and lower latitude ice sheets present at that time. From about 7000 years ago, sea level rose much more slowly. Over the last two millennia up until the 19th century, the little available evidence indicates the rate of global sea-level rise was less than a few tenths of a millimetre per year (Lambeck et al., 2004; Kemp et al., 2009).

From the 19th century to the present, the few available long-term tide gauge records (Woodworth, 1990), evidence from salt marshes (Kemp et al., 2009; Donnelly et al., 2004; Gerhels et al., 2005, 2006, 2008), and the available global sea-level estimates (Church and White, 2006, in press; Jevrejeva et al.,

2006, 2008; Woodworth et al., 2009, 2011) all indicate an increase in the rate of rise.

3.6.3.2 Current Sea Level Variability and Change

ENSO has a major influence on sea levels across the Pacific, as illustrated in Figure 3.20. During La Niña events, strengthened trade winds push more water toward the west resulting in a higher than normal sea surface in the western tropical Pacific, and lower than normal levels in the east. Conversely, during El Niño events, weakened trade winds are unable to maintain the normal gradient of sea level across the tropical Pacific, leading to a drop in sea level in the west and a rise in the east.

The influence of ENSO can be seen at individual island locations in the PCCSP region. The in situ and satellite observations of sea level indicate interannual variations of over 200 mm. These observed sea levels have been plotted along with reconstructed sea levels over the period from 1950 to 2009 in Figure 3.21. (Reconstructed sea level uses advanced statistical techniques to combine contemporary tide gauge and satellite sea-level measurements to estimate pre-satellite sea level from tide gauge measurements alone. Section 2.2; Church et al. 2004, 2006). In this equatorial region, the in situ

and satellite observations of sea level agree well with each other and the reconstructed sea levels.

As well as the influence of ENSO and other natural variability, sea level is also rising globally (Figure 3.22) and in the PCCSP region. The satellite altimeter record from 1993 to the present indicates that global averaged sea level has been rising at 3.2 ± 0.4 mm per year (Cazenave and Llovel, 2010; Church and White, in press). While in situ sea-level measurements do not have the same spatial coverage as the altimeter data, they can be used to make estimates of global averaged and regional sea-level variability and rise (Church and White, 2006, in press; Jevrejeva et al., 2006, 2008; Church et al. 2004, 2006). These estimates confirm the satellite altimeter record and indicate that global averaged sea level has been rising at about 1.7 ± 0.2 mm per year since 1900 (Church and White, in press). Together with other data, they also indicate the rate of rise has increased from the 19th to the 20th century (Bindoff et al., 2007) and during the 20th century (Church and White, 2006, in press; Jevrejeva et al., 2006).

Woodworth et al. (2009) considered the estimates of global averaged sea level and also the distribution of individual records around the globe. The two most prominent features were an increase in the rate of rise around the 1930s, and a decrease

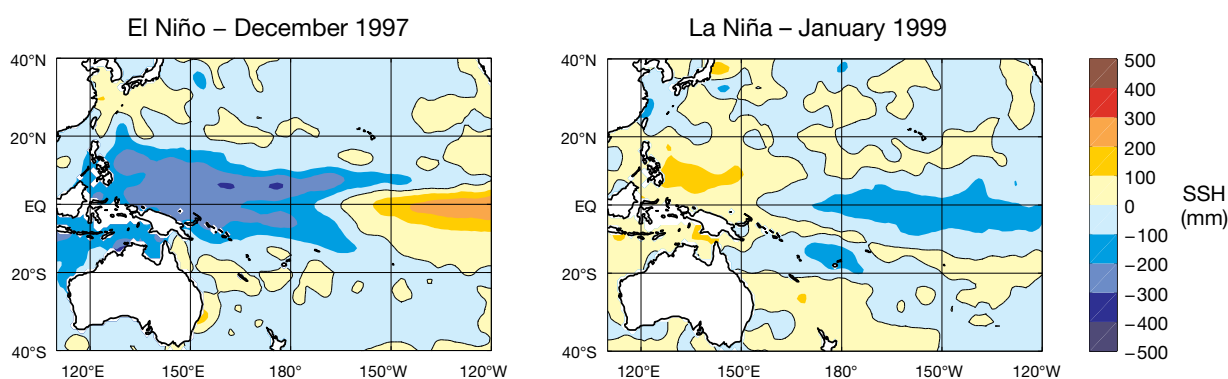


Figure 3.20: Sea-surface height variations relative to the long-term average (mm) across the Pacific during the December 1997 El Niño and January 1999 La Niña events. These are monthly averages from the satellite altimeter observations from 1993 to the present.

in the 1960s, which Houston and Dean (2011) considered in a subset of the global data. Major volcanic eruptions result in additional aerosol loading in the stratosphere and as a result some of the incoming solar radiation is reflected back to space leading to a short-term (a few years for the atmosphere) cooling of the Earth. The oceans also cool but have a substantially longer recovery time. The net effect is that the rate of rise

since the 1960s would most likely have been larger if it were not for the impact of major volcanic eruptions in 1963, 1982 and 1991 (Church et al., 2005; Gregory et al., 2006). Also, the additional storage of water in dams (Chao et al., 2008) has slowed the rate of sea-level rise, although this has been partly offset by the depletion of ground water. It is not yet known whether the faster rate of increase since 1993 is due to decadal

variability or a further acceleration in the long-term trend. Models indicate the recovery of the ocean from the eruption of Mount Pinatubo in 1991 would increase the rate of sea-level rise by about 0.6 mm per year. There is increasing evidence that the contribution to sea level due to mass loss from Greenland and Antarctica has increased over the past two decades (Velicogna, 2009; Rignot et al., 2011).

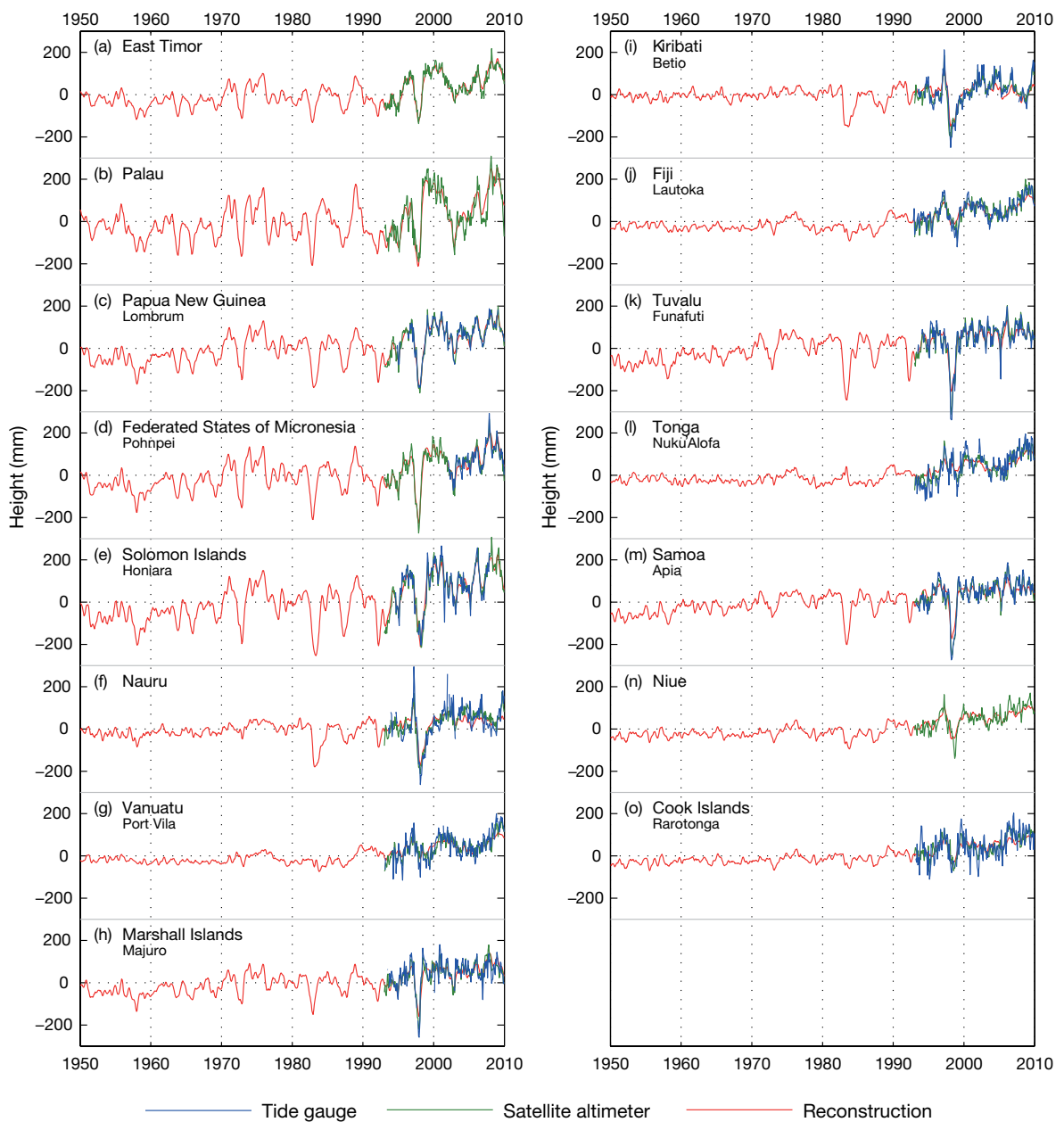


Figure 3.21: Time series of monthly tide gauge data (blue) from the South Pacific Sea Level and Climate Monitoring Project (where available), satellite altimeter data (green, from 1993) and reconstructed (red) sea levels using both sources of data, for PCCSP Partner Countries (based on methods in Church et al., 2006).

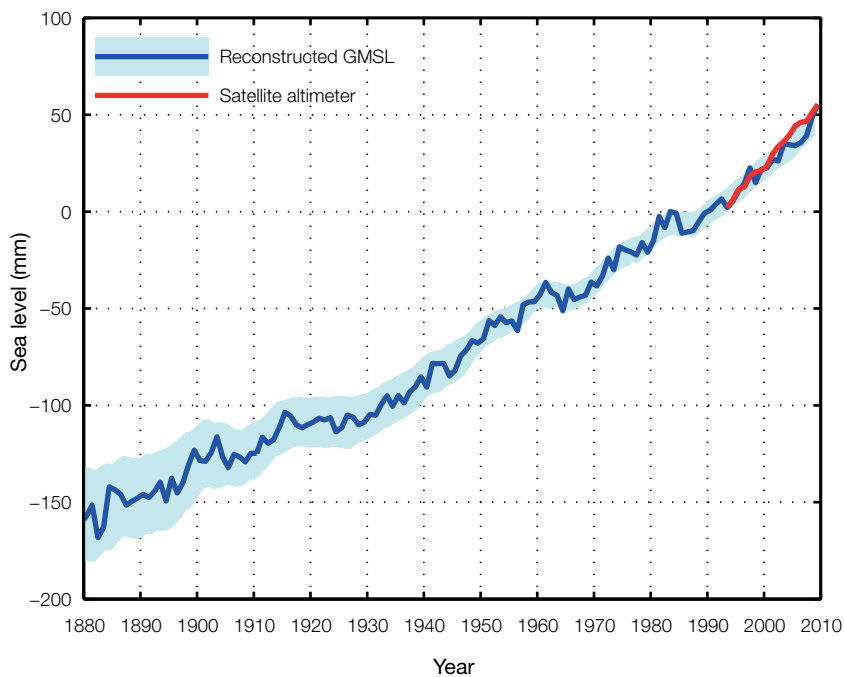


Figure 3.22: Annual global averaged sea level from 1880 to 2009 estimated from coastal and island sea-level data (blue) and from the satellite-altimeter data since 1993 (red). The one standard deviation uncertainty estimates plotted about the low passed (smoothed) sea level are indicated by the shading. The sea level estimated from the coastal and island data has an arbitrary datum and for convenience is set to zero in 1990. The altimeter data is set to the same value as the in situ data at the start of the satellite record in 1993 (following Church and White, in press).

Over the short period from 1993 to 2009, both the altimeter and in situ data indicate a higher than global average rate of rise in the western Pacific and eastern Indian Oceans, up to about three times the global average (Figure 3.23). However, because of the strong influence of ENSO and decadal variability on sea level in the region, this higher rate of rise is not necessarily representative of a longer time span. Merrifield (2011) argues that the high rates of sea-level rise in the western Pacific are a result of an intensification of the easterly trade winds across the tropical Pacific Ocean. For a longer time span, Church et al. (2006) examined the tide gauge records in the region and found the rate of relative sea-level rise (ocean relative to the land) was in the range -0.6 ± 0.5 mm per year to 6.7 ± 0.8 mm per year over varying time spans. Some of these records are likely to be affected by poorly known vertical land motions and poorly determined decadal variability.

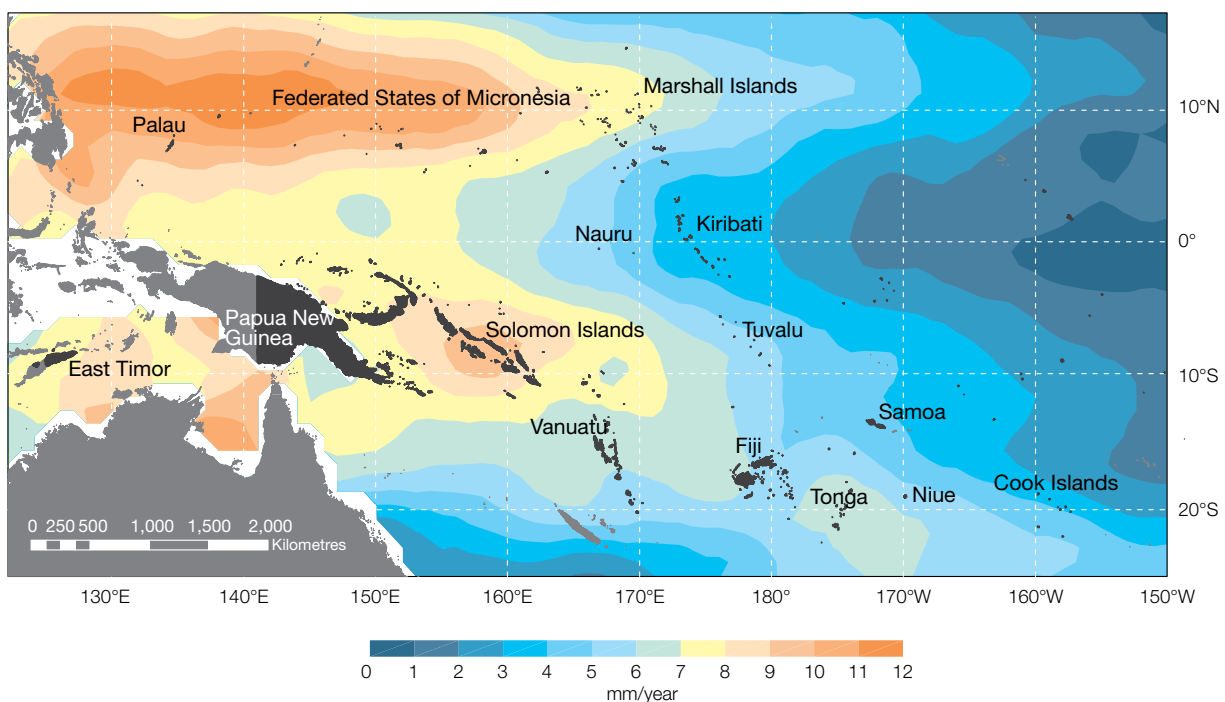


Figure 3.23: The regional distribution of sea-level rise measured by satellite altimeters from January 1993 through December 2009.

Trends in extreme sea level were analysed by Woodworth and Blackman (2004) at 141 tide gauges across the globe since 1975, including around 20 gauges in the tropical Pacific. By modifying the background state, rising sea levels and ENSO have a strong influence on the occurrence of extreme sea levels. Woodworth and Blackman (2004) showed that extreme sea levels are positively correlated with the SOI at tide gauges in the western tropical Pacific west of 180°, while gauges on the equator to the east of this are negatively correlated with the SOI. Menendez and Woodworth (2010) used sea-level records from 258 tide gauges across the globe, including over two dozen in the tropical Pacific, and found similar results. Hence, extreme high sea levels are more probable in the western Pacific (approximately to the west of 180°) during La Niña events, while to the east of 180° they are more probable during El Niño events. These relationships have been investigated in detail for the US-affiliated states (Guam, Palau, the Northern Mariana Islands, the Marshall Islands, the Federated States of Micronesia, and American Samoa) by Chowdhury et al. (2007, 2010) who noted that prediction of ENSO events can be used in early warning systems for sea-level extremes in the region.

For the highest 1% of sea levels, there are positive trends over decadal periods in most tide gauge records analysed (Woodworth and Blackman, 2004). These trends are similar to trends in mean sea level, leading to the conclusion that changes in mean sea level, and not changes in storminess, are driving current trends in extreme sea levels. Using two metrics for extreme sea levels, the 99th percentile sea level and the 50-year return period, Menendez and Woodworth (2010) also found that there has been an increasing trend in extreme sea levels globally, including in the PCCSP region, which has been more pronounced since the 1970s, and this trend is consistent with trends in mean sea level.

3.6.4 Ocean Circulation

A number of multi-decadal changes in ocean circulation have been observed in the Pacific region. As discussed in Section 3.4.6, there has been a poleward movement and acceleration of the sub-tropical westerlies over recent decades, associated with a more positive Southern Annular Mode. Dynamical arguments suggest that these wind changes should result in an increase in the strength of the South Pacific oceanic sub-tropical gyre. Such changes have indeed been identified in recent decades, via both in situ observations of ocean currents and

satellite altimetry, which can be used to infer large-scale circulation patterns (Roemmich et al., 2007). However, the observational record is short, making trends sensitive to natural variability. These changes have also been found in 20th century simulations from most climate models that include interactive atmosphere and ocean components (Cai et al., 2005; Saenko et al., 2005).

As noted earlier, there appears to have been a weakening of the Walker Circulation and associated equatorial trade winds since 1975 (Vecchi et al., 2006; Zhang and Song, 2006; Power and Smith, 2007; Power and Kocuiuba, 2010, in press), which might be expected to have had some influence on equatorial currents. Time series of currents are available from the array of instruments moored in discrete locations along the equatorial Pacific Tropical Atmosphere Ocean moorings (Hayes et al., 1991). These data confirm that large year-to-year variations in the strength of the sub-surface Equatorial Undercurrent (Figure. 2.13) is closely linked with changes in the overlying trade winds (Izumo, 2005). However, a discernable long-term trend is yet to be detected. At 110°W there is a small but statistically significant decrease in the strength of the surface South Equatorial Current but no significant trend is seen further west at 140°W.

3.6.5 Ocean Acidification

The ocean is a major sink for anthropogenic carbon dioxide (CO_2) and takes up about one quarter of the annual CO_2 emissions that result from human activities (Sabine et al., 2004; Le Quere et al., 2009). The CO_2 taken up by the ocean reacts in water and causes a decrease in the pH of the seawater that is referred to as ocean acidification. The pH change is accompanied by an increase in the concentration of total dissolved inorganic carbon, and a decrease in the dissolved carbonate ion concentration of the seawater (Feely et al., 2004). The decrease in dissolved carbonate ion concentrations causes a lowering of the seawater saturation states of the biogenic forms of calcium carbonate (aragonite, calcite and high magnesium calcite) that are secreted as shells or skeletal material by many key species in marine ecosystems (Feely et al., 2004).

The changes in the carbonate saturation states and in the pH of seawater predicted to occur this century have the potential to severely disrupt the health and sustainability of reef ecosystems (Guinotte and Fabry, 2008). While only a small number of species have been grown experimentally under high CO_2 conditions to mimic the acidification effects expected this century, evidence indicates that changes in carbonate saturation states may eventually lead to a condition where processes that act to degrade reefs (bioerosion, dissolution, storm damage) overcome the capacity of corals and other calcifiers to grow and maintain a healthy reef ecosystem (Manzello et al., 2008; Silverman et al., 2009). The reduction in seawater pH may also influence the lifecycle of marine organisms by altering long-term

metabolic function, reproduction and growth, although the sensitivity to these changes is not well known (Fabry et al., 2008; Guinotte and Fabry, 2008; Munday et al., 2009; Munday et al 2010). Other stressors, like ocean warming, are likely to add to the ecosystem response (Anthony et al., 2008; Hoegh-Guldberg et al., 2007).

Since pre-industrial times, the pH of global surface waters is estimated to have declined by about 0.1 units, representing about a 30% increase in the hydrogen ion concentration (Feely et al., 2009). Observations made since the early 1990s in the

sub-tropical North Pacific Ocean (Figure 3.24) show surface water pH decreases as the partial pressure of CO_2 ($p\text{CO}_2$) in the surface water increases as a result of CO_2 uptake driven by increasing concentrations of atmospheric CO_2 . The same data also show a long-term decline in the seawater saturation states of the biogenic carbonates, aragonite and calcite. The saturation states are the product of the concentrations of dissolved calcium and carbonate ion concentrations in seawater, divided by the solubility products for calcite and aragonite, respectively.

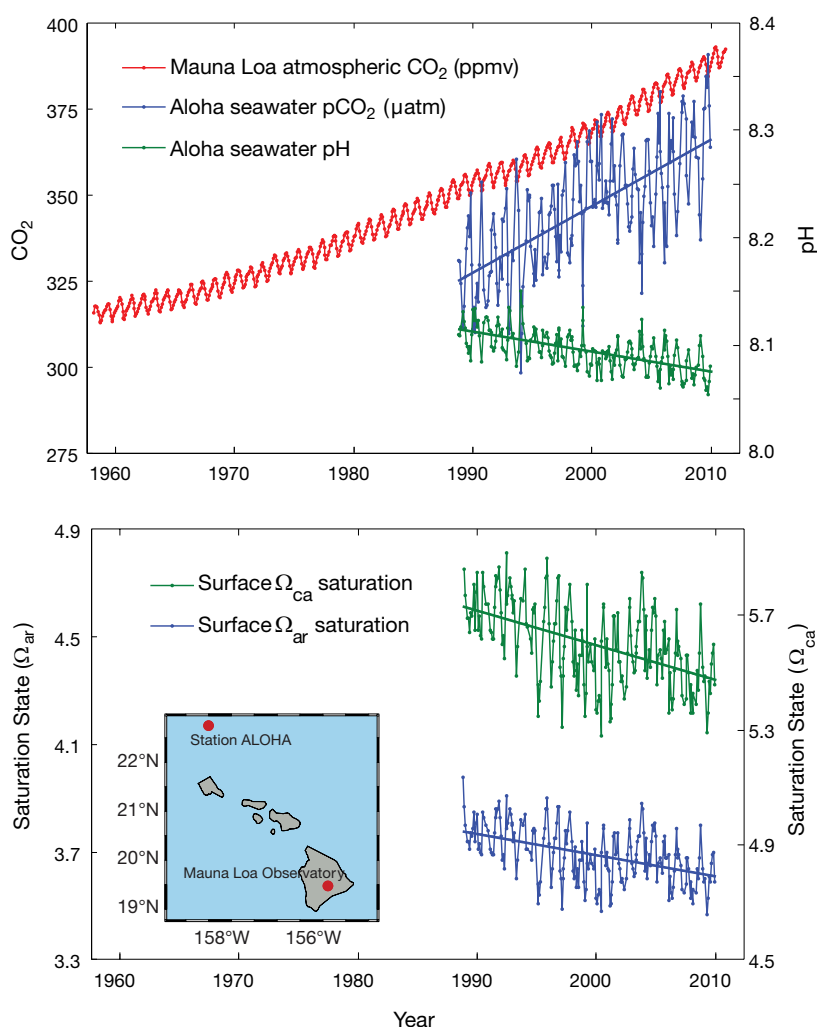


Figure 3.24: (Top) Atmospheric CO_2 measured at Mauna Loa Observatory (ppmv), and surface ocean pH and $p\text{CO}_2$ (μatm) at the Hawaii Ocean Time Series site, Station ALOHA, in the sub-tropical North Pacific Ocean. (Bottom) Seawater calcite and aragonite saturation state data for surface waters at Station ALOHA (Adapted from: Dore et al., 2009 and Feely et al., 2009).

Tropical reef-building corals secrete calcium carbonate as aragonite and tend to show a reduction in calcification at lower seawater aragonite saturation states (Langdon and Atkinson, 2005). Aragonite saturation states above 4 are considered optimal conditions for healthy coral reef ecosystems, with values below 3.5 becoming increasingly marginal for supporting healthy coral reef growth (Guinotte et al., 2003).

Data collected in the Pacific region as a part of the Joint Global Ocean Flux Study/World Ocean Circulation Experiment CO₂ survey allow estimates to be made of the aragonite saturation states of seawater in the pre-industrial era and in the 1990s. In pre-industrial times, the saturation state values were above 4 throughout most of the sub-tropical and tropical Pacific Island region, apart from a small equatorial band east of 150°W (Figure 3.25, top). By the mid 1990s, the uptake of anthropogenic CO₂ had resulted in a widespread decline in the aragonite saturation state, with values slightly above 4 only found in the region of the South Equatorial Current and in the western Pacific (Figure 3.25, bottom). Values of aragonite and other carbonate saturation states have continued to decline since the 1990s and only the surface waters of the South Equatorial Current now have aragonite saturation states that remain at or slightly above values of 4.

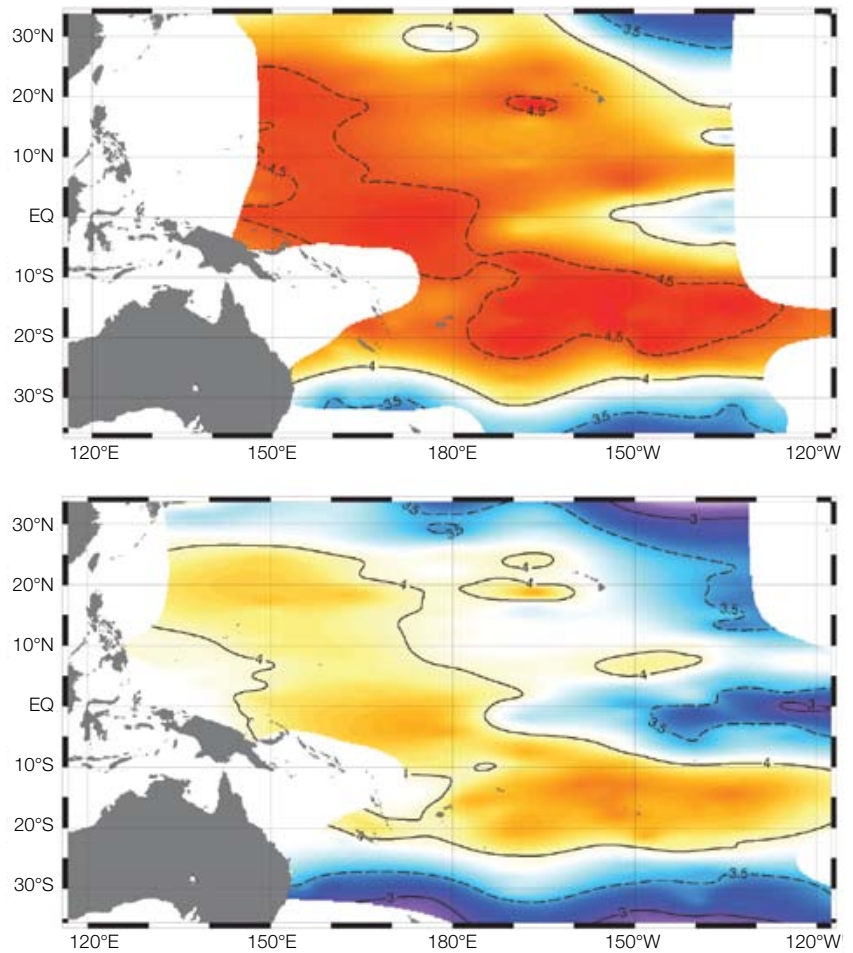


Figure 3.25: (Top) Seawater aragonite saturation state values calculated for the pre-industrial period (about 1765) using GLODAP data on dissolved inorganic carbon parameters (Lamb et al., 2002), including estimates of anthropogenic CO₂ (Sabine et al., 2004). (Bottom) The seawater aragonite saturation state calculated for JGOFS/WOCE CO₂ survey data collected in the 1990s (Data source: GLODAP data base, Carbon Dioxide Information Analysis Center, Oak Ridge, Tennessee, <http://cdiac.ornl.gov/oceans/glodap/>).